



NRL/FR/7322--03-10,055

Application of a Shelf-Scale Model to Wave-Induced Circulation: Rip Currents

MARK COBB
CHERYL ANN BLAIN

*Ocean Dynamics and Prediction Branch
Oceanography Division*

May 30, 2003

Approved for public release; distribution is unlimited.

REPORT DOCUMENTATION PAGE

Form Approved
OMB No. 0704-0188

Public reporting burden for this collection of information is estimated to average 1 hour per response, including the time for reviewing instructions, searching existing data sources, gathering and maintaining the data needed, and completing and reviewing this collection of information. Send comments regarding this burden estimate or any other aspect of this collection of information, including suggestions for reducing this burden to Department of Defense, Washington Headquarters Services, Directorate for Information Operations and Reports (0704-0188), 1215 Jefferson Davis Highway, Suite 1204, Arlington, VA 22202-4302. Respondents should be aware that notwithstanding any other provision of law, no person shall be subject to any penalty for failing to comply with a collection of information if it does not display a currently valid OMB control number. PLEASE DO NOT RETURN YOUR FORM TO THE ABOVE ADDRESS.

1. REPORT DATE (DD-MM-YYYY) 30-05-2003		2. REPORT TYPE Formal		3. DATES COVERED (From - To)	
4. TITLE AND SUBTITLE Application of a Shelf-Scale Model to Wave-Induced Circulation: Rip Currents				5a. CONTRACT NUMBER	
				5b. GRANT NUMBER	
				5c. PROGRAM ELEMENT NUMBER	
6. AUTHOR(S) Mark Cobb and Cheryl Ann Blain				5d. PROJECT NUMBER 73-6727-03	
				5e. TASK NUMBER	
				5f. WORK UNIT NUMBER	
7. PERFORMING ORGANIZATION NAME(S) AND ADDRESS(ES) Naval Research Laboratory Oceanography Division Stennis Space Center, MS 39529-5004				8. PERFORMING ORGANIZATION REPORT NUMBER NRL/FR/7322--03-10,055	
9. SPONSORING / MONITORING AGENCY NAME(S) AND ADDRESS(ES) Office of Naval Research 800 North Quincy St. Arlington, Virginia 22217-5560				10. SPONSOR / MONITOR'S ACRONYM(S) ONR	
				11. SPONSOR / MONITOR'S REPORT NUMBER(S)	
12. DISTRIBUTION / AVAILABILITY STATEMENT Approved for public release; distribution is unlimited.					
13. SUPPLEMENTARY NOTES					
14. ABSTRACT Wave-induced rip currents on barred planar beaches are simulated using ADCIRC-2DDI, a two-dimensional finite-element hydrodynamic model. Surface wave stress gradients, determined from REF/DIF1, a phase-resolving monochromatic wave model that simulates refraction, diffraction, and wave breaking, are used to force the ADCIRC model. The rip current circulation on an ideal barred beach, approximately 1 km ² in area with a single channel in the center of its alongshore bar, is investigated. Solutions for steady and unsteady circulation are examined by considering the relative influence of lateral mixing and nonlinear bottom stress. Shear-induced vortices are produced by the unsteady rip current, causing it to move in the alongshore and cross-shore directions. ADCIRC-2DDI solutions for the circulation on the ideal beach are found to be qualitatively similar to actual rip currents observed in field and laboratory studies. Good agreement is found between the steady state ADCIRC-2DDI results and the time-averaged laboratory measurements for the water level and the currents. Finally, wave-current (w-c) interaction is simulated on the ideal barred beach by iteratively coupling ADCIRC-2DDI and REF/DIF1. Rip current-induced refraction and shoaling significantly modify the wave field, changing the circulation of the rip current.					
15. SUBJECT TERMS Nearshore circulation Wave processes on beaches Rip currents Wave-current interaction Hydrodynamics Numerical models					
16. SECURITY CLASSIFICATION OF:			17. LIMITATION OF ABSTRACT UL	18. NUMBER OF PAGES 31	19a. NAME OF RESPONSIBLE PERSON Mark Cobb
a. REPORT Unclassified	b. ABSTRACT Unclassified	c. THIS PAGE Unclassified			19b. TELEPHONE NUMBER (include area code) 228-688-4474

CONTENTS

INTRODUCTION.....	1
CIRCULATION AND WAVE MODELS.....	2
IDEAL BARRED BEACH	4
Steady State Circulation.....	4
Unsteady Circulation	10
SIMULATION OF A LABORATORY SCALE RIP CURRENT	13
Steady State.....	14
Unsteady State	19
Wave-current Interaction	19
CONCLUSION	24
ACKNOWLEDGMENTS.....	25
REFERENCES.....	26

APPLICATION OF A SHELF-SCALE MODEL TO WAVE-INDUCED CIRCULATION: RIP CURRENTS

INTRODUCTION

As the number of people living in coastal areas increases, the ability of scientists and engineers to understand and predict nearshore circulation patterns becomes more important. Because nearshore circulation affects sediment transport, pollutant transport, and the biology of the coastal environment, it is relevant to the safety of the coastal inhabitants as well as the stability of the nearshore environment (e.g., beach erosion). These issues have been examined in the past with highly simplified models, but in recent years, increasingly more sophisticated wave and hydrodynamic models have been employed (Ozkan-Haller and Kirby 1999; Slinn et al. 1998). The motivation behind this study is to apply a fully developed and thoroughly tested shelf-scale circulation model to the problem of simulating nearshore wave-induced circulation. A previous report, Blain and Cobb (2002; hereafter referred to as BC02), addressed the issues (e.g., grid resolution, specification of various model parameters) pertaining to the application of the ADCIRC coastal shelf-scale circulation model (Luettich et al. 1992; Westerink et al. 1994a) to wave-induced circulation on plane and barred beaches. The effects of varying the lateral mixing and nonlinear bottom friction coefficients on the nearshore circulation were also investigated. Model-data comparisons demonstrated that ADCIRC was able to reproduce alongshore current profiles that were measured at several different field sites.

This report focuses on applying ADCIRC to the more complex nearshore phenomena of rip currents. It should be emphasized that ADCIRC is not intended as a replacement for models such as SHORCIRC (Van Dongeren and Svendsen 2000) that are specifically targeted at simulating nearshore circulation. Instead, the results of ADCIRC should be viewed as a reasonable first approximation to the actual nearshore circulation with the potential of providing boundary and/or initial conditions for a true nearshore model. Values are chosen for the ADCIRC model parameters that produce realistic circulation patterns, but no attempt is made to actually calibrate the ADCIRC model parameters. In fact, the range of parameter values is rather robust when compared to the range of parameter values used by BC02 for alongshore current simulations.

Coastal scientists have observed rip currents for many years (Shepard et al. 1941; McKenzie 1958), but the driving mechanism behind rip current circulation is still an issue of debate and discussion. Currently, two distinct scenarios for rip current generation are proposed: 1) via wave interaction, which includes wave-wave and wave-current (w-c) interaction (Bowen 1969; LeBlond and Tang 1974; Dalrymple 1975), or 2) via bathymetric variations, such as rip channels on barred beaches, that result in complex wave set-down/set-up patterns (Dalrymple 1978). Laboratory experiments have been performed over the last decade to simulate coastal rip currents on barred beaches with rip channels (Hamm 1992; Haller et al. 1997; Drønen et al. 1999; Haller and Dalrymple 1999) and recent numerical modeling studies have focused on rip currents generated in this manner (Haas et al. 1998; Chen et al. 1999; Yu and Slinn 2001 in press).

This report is divided into four main sections; the first section focuses on the ADCIRC model, and the remaining sections focus on its application to rip currents. In the first section, brief descriptions are given of the 2D, depth-integrated version of ADCIRC (ADCIRC-2DDI) and the approach used to force the model with waves. REF/DIF1 (Kirby and Dalrymple 1994), the linear, monochromatic, phase-resolving wave model used to determine the wave forcing, is described as well. Both one-way and two-way coupling of ADCIRC and REF/DIF1 are detailed. In the last section of this report, two-way (or iterative) coupling is used to simulate w-c interaction.

Wave-driven rip currents are simulated on an ideal barred beach with a single rip channel in the second section of this report. The resulting sea surface elevations and currents are examined in the context of their driving mechanisms and compared to field studies and recent laboratory experiments. The stability of this rip current is investigated through a parameter study of the lateral mixing and nonlinear bottom friction coefficients. In order to make comparisons to available rip current data, the laboratory experiment of Haller and Dalrymple (1999), consisting of an 11 m by 18.2 m wave tank containing a barred beach with two rip channels, is simulated in the third section of this report. The stability of this rip current system is also investigated by reducing the influence of lateral mixing.

The last section of this report presents a preliminary study of w-c interaction. This section demonstrates how ADCIRC can be used in a coupled model scheme to simulate w-c interaction. Currently there are no fully developed shelf-scale models that incorporate w-c interaction, thus coupling a shelf-scale hydrodynamic model with a wave model is the best (albeit transitional) solution to this problem. The effect of w-c interaction on the rip current of the ideal barred beach is investigated by iteratively coupling ADCIRC-2DDI and REF/DIF1. In the previous study of longshore currents by BC02, the interaction of the wave field with the currents was ignored and assumed to be negligible, but for the case of a rip current, significant w-c interaction is expected. A strong rip current that opposes incident waves can induce shoaling, refraction, and even wave breaking. This w-c interaction study does not address in detail the issues involved in coupling the two models. Instead, the focus is on the qualitative changes that occur in the rip current as a result of w-c interaction.

CIRCULATION AND WAVE MODELS

Sea surface elevation and coastal currents are modeled using the fully nonlinear, 2-D, barotropic hydrodynamic model ADCIRC-2DDI. The ADCIRC (ADvanced CIRCulation Model for Shelves, Coasts and Estuaries) model, developed by Luettich et al. (1992) and Westerink et al. (1994a), has a successful history of tidal and storm surge prediction in coastal waters and marginal seas (e.g., Blain et al. 1994; Kolar et al. 1994; Westerink et al. 1994b; Blain et al. 1998). The depth-integrated shallow water equations, derived through vertical integration of the three-dimensional mass and momentum balance equations subject to the hydrostatic assumption and the Boussinesq approximation, form the basis of the ADCIRC-2DDI model. Tidal, wind, and Coriolis forcing effects are neglected in order to isolate wave-driven nearshore flows. A spatially variable surface stress forcing is determined from the radiation stress (S_{xx} , S_{yy} , S_{xy} , S_{yx}) gradients of the wave field (Longuet-Higgins and Stewart 1964) obtained from the REF/DIF1 wave model. The simplified nonconservative primitive equations are

$$\frac{\partial \zeta}{\partial t} + \nabla_{xy} \cdot (H\mathbf{v}) = 0 \quad (1)$$

$$\frac{\partial \mathbf{v}}{\partial t} + \mathbf{v} \cdot \nabla_{xy} \mathbf{v} = -\nabla_{xy} (g\zeta) + \frac{M_{xy}}{H} + \frac{\tau_{sxy}}{\rho_0 H} - \frac{\tau_{bxy}}{\rho_0 H} \quad (2)$$

$$\tau_{sx} = -\left(\frac{\partial S_{xx}}{\partial x} + \frac{\partial S_{yx}}{\partial y}\right) \quad (3)$$

$$\tau_{sy} = -\left(\frac{\partial S_{yy}}{\partial y} + \frac{\partial S_{xy}}{\partial x}\right), \quad (4)$$

where t represents time, x, y are the Cartesian coordinate directions, ζ is the free surface elevation relative to the geoid, \mathbf{v} is the depth-averaged horizontal velocity vector, $H = \zeta + h$ is the total water column depth, h is the bathymetric depth relative to the geoid, g is the acceleration due to gravity, ρ_0 is the reference density of water, M_{xy} is the horizontal momentum diffusion/dispersion, τ_{sx} and τ_{sy} are the applied horizontal free surface stresses, and τ_{bxy} is the horizontal bottom stress vector. This set of equations is considered to be time-averaged over a wave period. Bottom stress terms are parameterized using the standard nonlinear quadratic friction law:

$$\tau_{bxy} = C_f \rho_0 (U^2 + V^2)^{1/2} \mathbf{v}, \quad (5)$$

where C_f is the nonlinear bottom friction coefficient. The lateral mixing due to diffusion/dispersion is:

$$M_{xy} = E_h (\nabla_{xy}^2 (H\mathbf{v})), \quad (6)$$

where E_h is the horizontal eddy viscosity coefficient for momentum diffusion/dispersion (Kolar and Gray 1990).

The wave field used to force the ADCIRC-2DDI hydrodynamic model is derived from the linear monochromatic wave model, REF/DIF1 (Kirby 1986; Kirby and Dalrymple 1994). The monochromatic nature of this model allows propagation of a single wave frequency over irregular bathymetry. The REF/DIF1 model is a phase-resolving, frequency domain model based on the parabolic approximation to the mild-slope equation for water wave propagation. REF/DIF1 uses a breaking criterion of $H > 0.78h$ (H is the wave height and h is the water depth) and a dissipation model to determine if wave breaking will occur (Kirby and Dalrymple 1994). REF/DIF1 has the capability of using sea surface elevations and currents as input for the calculation of the wave field.

ADCIRC-2DDI and REF/DIF1 are one-way coupled in all but the last section of this report. Wave heights and directions computed by the REF/DIF1 wave model are interpolated onto the computational nodes of the finite element grid and radiation stress gradients are then determined for each node. The REF/DIF1 wave field is static and does not change in response to the current field. It should be pointed out that initially during an ADCIRC simulation there is a 'spin-up' phase. During the spin-up phase the surface stress terms are gradually increased in strength through a ramp function to their actual values. The spin-up phase helps avoid exciting significant transient modes that may occur when the simulation begins. In order to investigate the changes in the rip current circulation in response to a circulation-modified wave field, wave-current interaction is incorporated by iteratively coupling ADCIRC and REF/DIF1 in the last section of this report. The sea surface elevations and currents of ADCIRC-2DDI are used by REF/DIF1 to compute a new wave field, which is then used to recalculate the nodal radiation stress gradients. The ADCIRC model is initially run without two-way coupling for a time interval sufficient to obtain a steady circulation state. After this initial spin-up of the model, two-way coupling is activated and ADCIRC is run forward for a brief time interval (several seconds in the case of the ideal

barred beach), driven by a new static wave field. At the end of this time interval a new wave field is computed by REF/DIF1 and the ADCIRC simulation proceeds with a new radiation stress field as before.

IDEAL BARRED BEACH

Steady State Circulation

The first case examined is a 750 m by 1500 m barred beach with a slope of 0.009, shown in Fig. 1. The bar, with a cross-shore width of about 200 m, is located approximately 350 m offshore. A single channel, with a maximum alongshore width of 255 m, divides the bar at the center of the domain. Note that the center of the rip channel is identified at $y = 742.5$ m, creating a slight asymmetry in the length of the bars. The finite element mesh for this domain has 20301 computational nodes and resolves the bathymetry at 7.5 m with a regular grid of equally spaced nodes. A no-flow boundary is imposed at the shoreline, radiation boundary conditions are employed for the lateral boundaries, and a zero sea surface elevation is maintained at the offshore boundary. The dimensions of the beach are selected to minimize lateral boundary interaction and allow realistic seaward flow of the rip current. The wave height field shown in Fig. 2(a) results from normally incident waves that have a period of 10 s and an initial height of 1.0 m computed on a grid that has a resolution of 3.75 m. The values of these wave parameters are appropriate for coastal wave conditions that generate rip currents (Smith and Largier 1995). In addition, these values generate waves that break along the bars of the beach.

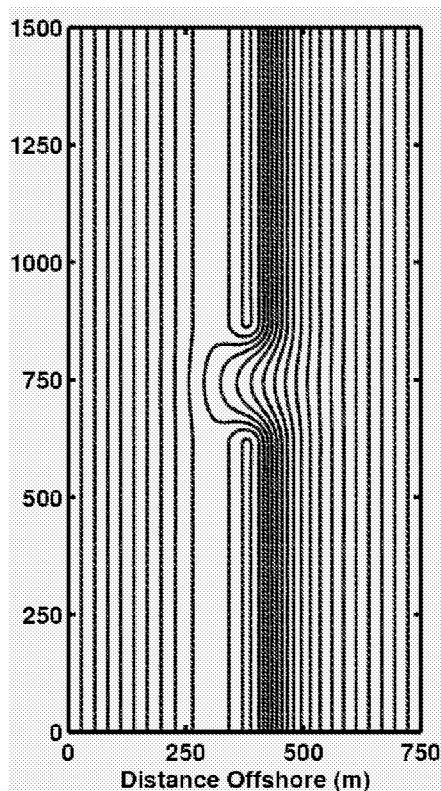


Fig. 1 — Bathymetry for the ideal barred beach. The bathymetric contour interval is 0.25 m.

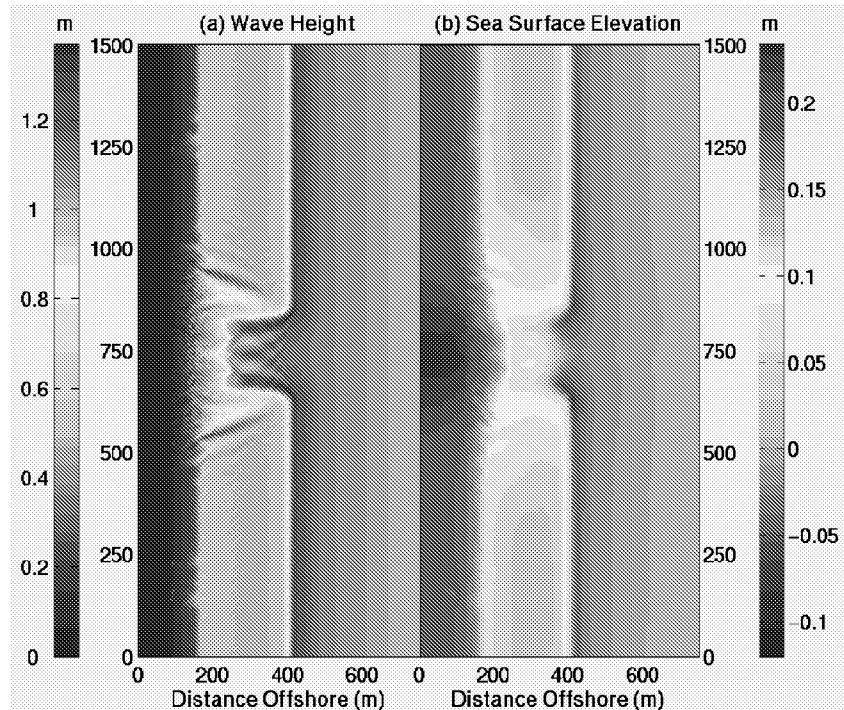


Fig. 2 — Ideal barred beach: (a) REF/DIF1 wave height field and (b) steady state sea surface elevations

A steady state circulation is obtained with a simulation time period of 14.4 h using a bottom friction coefficient, C_f , of 0.004 and a lateral mixing coefficient, E_h , of $2.0 \text{ m}^2/\text{s}$. A detailed discussion pertaining to the selection of these parameter values can be found in BC02. Although steady state conditions are probably unrealistic in nature, time-averaged mean current and sea surface elevation fields are described quite well by a steady state circulation pattern. Note that the values selected for C_f and E_h are similar to those used to obtain a steady alongshore current in BC02. The reasons for this similarity are discussed in a latter section of this report. A time step of 0.25 seconds is utilized to satisfy the Courant condition of the model (Westerink et al. 1994a).

The circulation of the ideal barred beach depends on the alongshore and cross-shore structure of the sea surface elevation. The sea surface elevation itself is determined to a great extent by the alongshore and cross-shore structure of the wave field. In the rest of this section the alongshore and cross-shore structure of the wave field, the sea surface elevation, and the current of the ideal barred beach are described in detail. The structure of the circulation seaward and shoreward of the bar will be examined as well. The rip current circulation of the ideal barred beach provides a clear picture of basic rip current circulation when bathymetric perturbations, other rip channels, and wave-current interaction are absent. As is apparent in the latter sections of this report, rip current circulation can become very complex in more realistic situations. A clear understanding of the ideal barred beach circulation makes it much easier to discern what is occurring in the more complex situations.

Cross-shore primary wave breaking occurs for this barred beach initially on the bars and later in the rip channel as shown in Fig. 2(a). This creates an alongshore variation in the wave set-down and set-up of the sea surface elevation (Fig. 2(b)), resulting in an alongshore pressure gradient directed towards the rip channel. This is the typical alongshore variation in sea surface height that is observed for rip currents on barred beaches that have channels (Sonu 1972; Dalrymple 1978). The set-down created by waves breaking on the bar also creates a shoreward directed pressure gradient on the seaward side of the bar.

The maximum set-down occurs in the vicinity of the channel at the end of each bar as seen from Fig. 2(b). This results in an offshore pressure gradient that is focused towards the rip channel.

The cross-shore primary wave breaking in the rip channel and cross-shore secondary wave breaking shoreward of the bar results in a cross-shore set-up at the shoreline as seen from Figs. 3(a) and 3(c). Figure 3(b) depicts the cross-shore bathymetry in the rip channel and on the bar and serves to locate the cross-shore sea surface elevation and wave height features with respect to the bar. The primary wave breaking in the rip channel is larger than the secondary breaking shoreward of the bar (Fig. 3(c)), resulting in a larger set-up at the shoreline (Fig. 3(a)). The alongshore variation in set-up at the shoreline, seen in Fig. 2(b), creates an alongshore pressure gradient directed away from the rip channel. Similar wave-induced set-up patterns on barred beaches have been observed by others in laboratory experiments and field studies (Haller et al. 1997; Drønen et al. 1999).

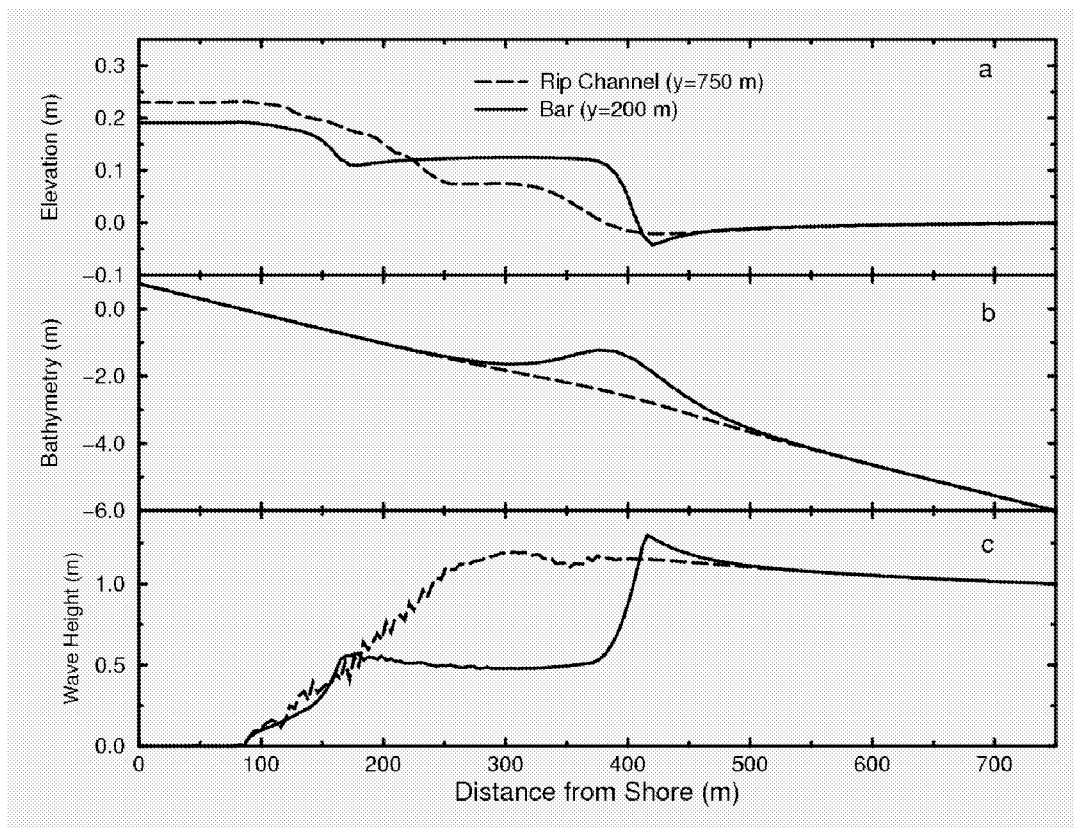


Fig. 3 — Ideal barred beach: Cross-shore transects on the bar ($y = 200$ m) and in the rip channel ($y = 750$ m) of the (a) steady state sea surface elevation, (b) bathymetry, and (c) wave height

Refraction and diffraction of waves in the vicinity of the rip channel result in alongshore and cross-shore variations of the wave field. The variation in the wave field on the shoreward side of the rip channel (Fig. 2(b)) creates, through set-up and set-down, complex alongshore and cross-shore sea surface elevation patterns. It is apparent from Fig. 2(b) that there is in fact a local maximum in the alongshore and cross-shore sea surface elevation located 300 m offshore in the rip channel. As seen from Fig. 3(a), the sea surface elevation increases significantly in this location *before* wave breaking occurs in the rip channel. This local maximum in the surface elevation results in an offshore directed pressure gradient. An in-depth discussion will follow later as to why this feature exists in the sea surface elevation.

The alongshore and cross-shore pressure gradients force water to flow into the rip channel on the shoreward and seaward sides of the bar (Fig. 4). The largest wave-induced set-down, on the seaward side of the rip channel at the end of each bar, creates shoreward directed feeder currents on both sides (alongshore direction) of the rip channel. The feeder currents, shown in Fig. 4, turn around in the rip channel because of the offshore directed pressure gradient and flow offshore as part of the rip current. It is apparent from Fig. 5(a) that the cross-shore rip current and feeder currents have similar magnitudes at the mouth of the rip channel 400 m offshore. The turning of the feeder currents is also apparent from Fig. 5(b) in which the alongshore current rapidly increases and then decreases in the rip channel as the rip current forms 300 m offshore. Shepard et al. (1941) and Sonu (1972) observed this type of circulation pattern in their field studies of rip currents.

Shoreward of the bar water flows in alongshore direction toward the rip channel, but as the current approaches the middle of the rip channel it diverges into seaward and shoreward flows about 300 m offshore (Fig. 4). The cross-shore current diverges and the alongshore current goes to zero in the rip channel around $x = 300$ m and $y = 750$ m as seen from Figs. 4, 5(a), and 5(b). It should also be pointed out that the cross-shore current is quite small in this region as well (Fig. 5(a)). The divergence in the current creates a stagnation point where the current goes to zero. The previously mentioned local maximum in the surface elevation, seen along the transect at $x = 300$ m in Fig. 5(c), is the location of the stagnation point. The shoreward flowing current ($x < 300$ m) is forced away from the rip channel by the alongshore pressure gradient near the shoreline. The fluid eventually circulates back to the rip channel due to the alongshore pressure gradient directed towards the rip channel. The result is the formation of large oppositely rotating eddies on both sides of the rip channel (Fig. 4). These eddies extend approximately 400 m in the alongshore direction on both sides of the rip channel. Haller et al. (1997) and Drønen et al. (1999) have observed this type of eddy formation (or secondary circulation) in laboratory experiments. In addition, smaller eddies exist within the large-scale eddy circulation. These smaller eddies are due in part to the complex patterns of the wave forcing field on the shoreward side of the rip channel.

Figure 6 plots alongshore-directed pressure and radiation stress gradients along a transect 300 m offshore that passes through the stagnation point in the alongshore direction. For the purpose of comparison, Fig. 6 also plots the sum of all the alongshore-directed forcing terms and the *scaled* sea surface elevation. It is apparent from Fig. 6 that the alongshore radiation stress gradients are balanced to a great extent by alongshore pressure gradients. The complex elevation patterns in the vicinity of the rip channel (Fig. 2(b)), that range from 200 m to 400 m in x and 500 m to 1000 m in y , can be better understood from this point of view. The structure of sea surface elevation in the vicinity of the rip channel is therefore due primarily to the rather complex wave field in this region (Fig. 2(a)). It also appears from Fig. 6 that the forces are not balanced in the vicinity of the stagnation point where the cross-shore current is diverging. The pressure gradients around $y = 700$ m and $y = 800$ m are larger than the radiation stress gradients creating a force imbalance. From symmetry arguments one would expect the converging alongshore currents to pile up water in the middle of the domain and create a stagnation point. The alongshore pressure gradient is therefore opposing not only the radiation stress gradient but also the force associated with inertial motion in the vicinity of the stagnation point.

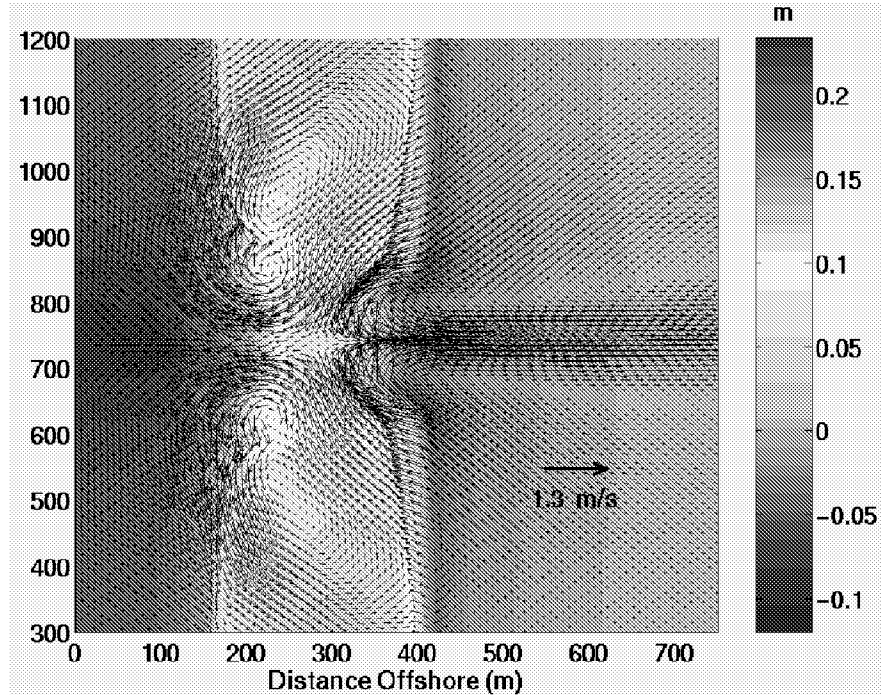


Fig. 4 — Ideal barred beach: Steady state sea surface elevations and currents between $y = 300$ and $y = 1200$ m. An arrow representing a 1.3 m/s current indicates the magnitudes of the current field vectors. Note: Only every other current vector of the current vector field is plotted.

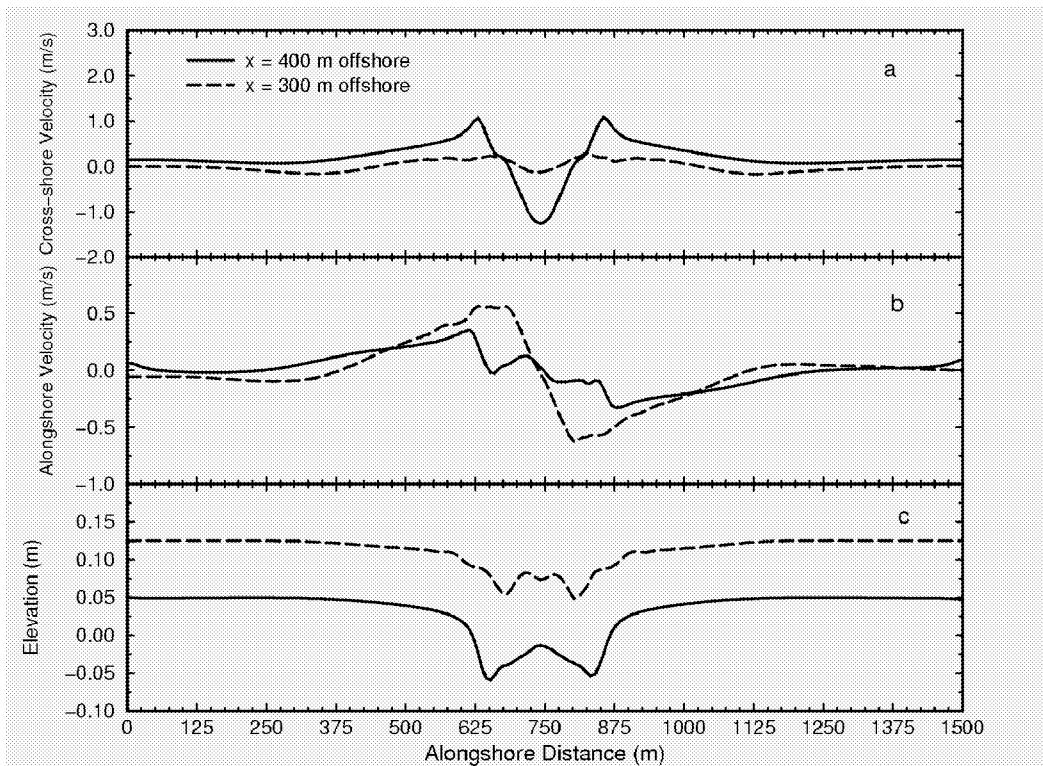


Fig. 5 — Ideal barred beach: Alongshore transects at $x = 300$ m and $x = 400$ m of the steady state (a) cross-shore current, (b) alongshore current, and (c) sea surface elevation

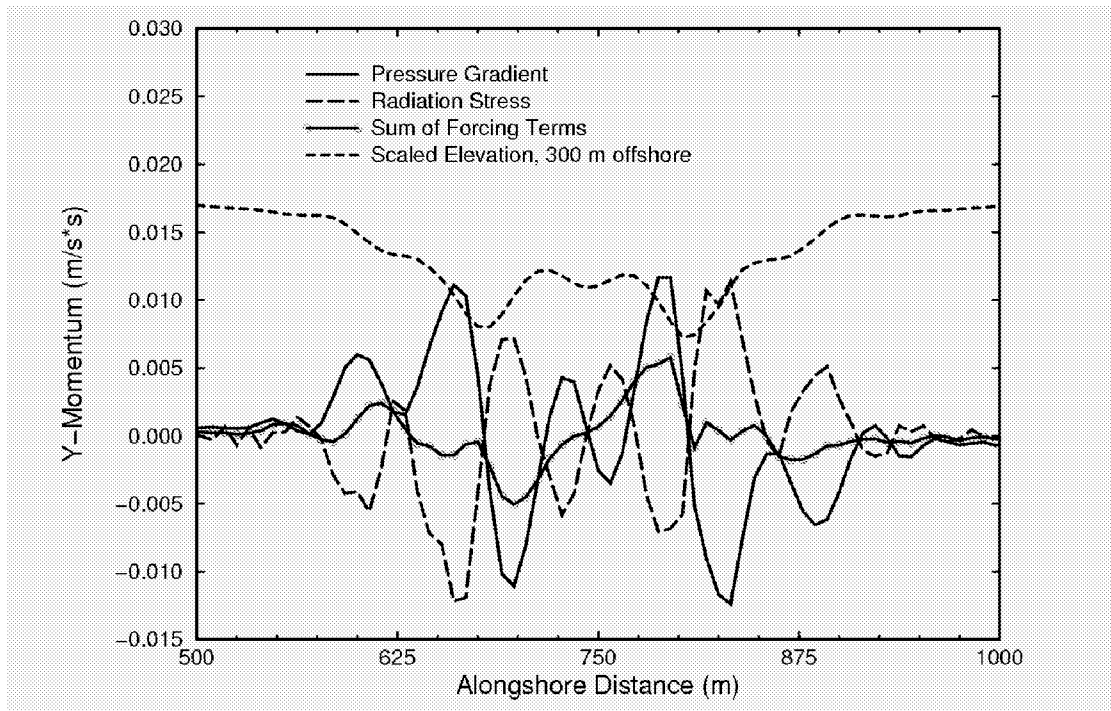


Fig. 6 — Ideal barred beach: Alongshore transects at $x = 300$ m of the steady-state, alongshore, directed-pressure gradient, radiation-stress gradient, and sum of all the alongshore directed forcing terms. The scaled steady-state elevation is also depicted in order to see the correspondence between it and the forcing terms.

Figure 7 plots cross-shore-directed pressure and radiation stress gradients along a cross-shore transect in the rip channel at $y = 750$ m; as was done in Fig. 6, the sum of the cross-shore-directed forcing terms and the *scaled* elevation are displayed in Fig. 7. The elevation at the stagnation point, located 300 m offshore, creates the offshore-directed pressure gradient seen in Fig. 7. This pressure gradient forces the shoreward flowing feeder currents, as previously discussed, to change direction and form the rip current. The inertial motion of the shoreward moving feeder currents, in addition to the alongshore inertial motion previously discussed, must also contribute to the cross-shore pressure gradient at the stagnation point. Stagnation points have been observed in laboratory studies by Haller et al. (1997) and Drønen et al. (1999) for rip currents produced using normally incident monochromatic waves.

About 420 m offshore, beyond the mouth of the rip channel, the pressure gradient in Fig. 7 becomes positive, opposing the rip current. The nonlinear bottom friction (not shown) and the shoreward flowing feeder currents (seen in Fig. 4) also oppose the rip current. As seen from Fig. 8(a) the rip current velocity reaches its maximum magnitude at the mouth of the rip channel located about 400 m offshore and then decreases in magnitude further offshore. Figure 8(b) provides a bathymetric reference for Fig. 8(a). The offshore rip current in this simulation extends about 350 m to the offshore boundary and does not go to zero as seen from Fig. 8(a). If the domain were larger the rip current would extend until its cross-shore velocity went to zero. The offshore velocity of the rip current is within the observed range of values for field studies with similar wave conditions (Shepard and Inman 1950; Smith and Largier 1995).

Note the existence of a narrow region between the rip current and feeder currents in which the current changes direction (Fig. 4). The shoreward flowing feeder currents are entrained by the offshore-directed rip current, causing the rip current to spread as it moves offshore. This entrainment process, which can lead to unsteady rip currents, is discussed further in the next section. Qualitatively, this behavior is similar to that of a viscous jet on a planar beach with friction (Joshi 1982; Haller and Dalrymple 1999). From Fig. 4 it is also apparent that the spreading of the rip current is approximately linear beyond 500 m.

Shepard et al. (1941) and Sonu (1972) observed the offshore spreading of jetlike rip currents in field studies.

Unsteady Circulation

Rip currents have been observed to change their direction and the intensity of their offshore fluid transport over relatively short periods of time. Field and laboratory studies suggest that eddies, which form on the sides of the rip current due to shear, contribute to this unsteadiness of the rip current (Shepard et al. 1941; Smith and Largier 1995; Haller et al. 1997). BC02 demonstrated that unsteady shear wave modes occur in the alongshore current of a planar beach when the lateral mixing and/or the nonlinear bottom friction coefficients are reduced below certain threshold values. A similar parameter study of these coefficients is performed for the ideal barred beach to determine a range of coefficient values that produce realistic circulation patterns. Acceptable values for the lateral mixing (0.5 to 2.0 m^2/s) and the nonlinear bottom friction (0.002 to 0.007) coefficients are found to be quite similar to those of BC02. The transition to an unsteady rip current occurs for values of the lateral mixing coefficient below approximately 2.0 m^2/s . This value is four times larger than the equivalent transition value for the unsteady alongshore current of the ideal planar beach (BC02). The alongshore current and the rip current do exhibit the same sensitivity to the value of C_f though, assuming that their differing sensitivities to the lateral mixing coefficient are taken into account.

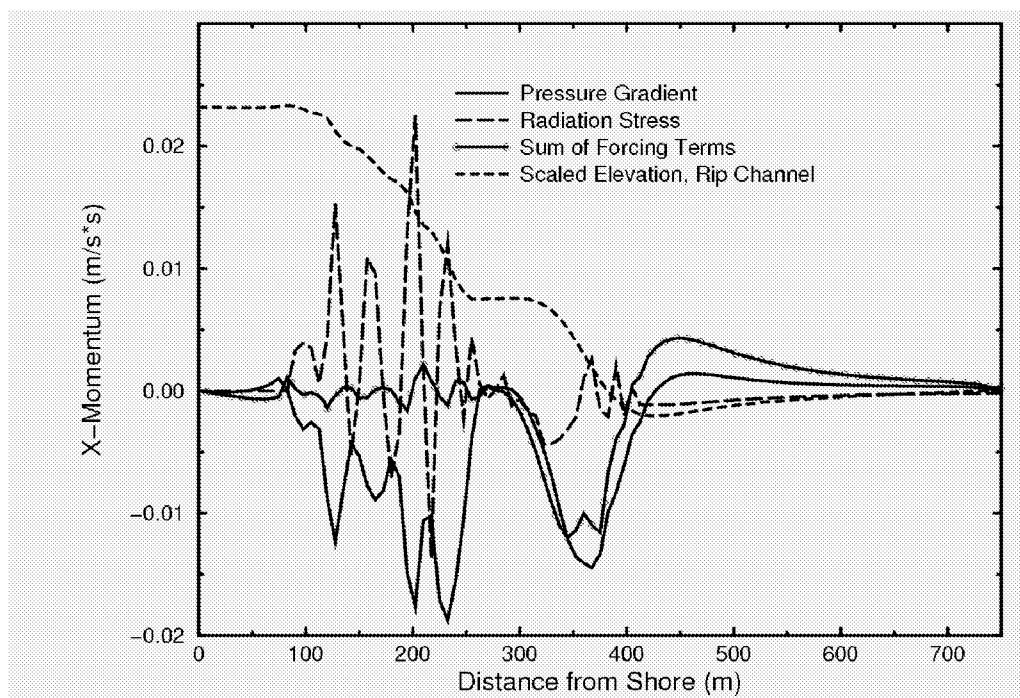


Fig. 7 — Ideal barred beach: Cross-shore transects along the rip channel ($y = 750$ m) of the steady-state, cross-shore-directed pressure gradient, radiation-stress gradient, and sum of all the cross-shore-directed forcing terms. The scaled steady-state elevation is also depicted in order to see the correspondence between it and the forcing terms.

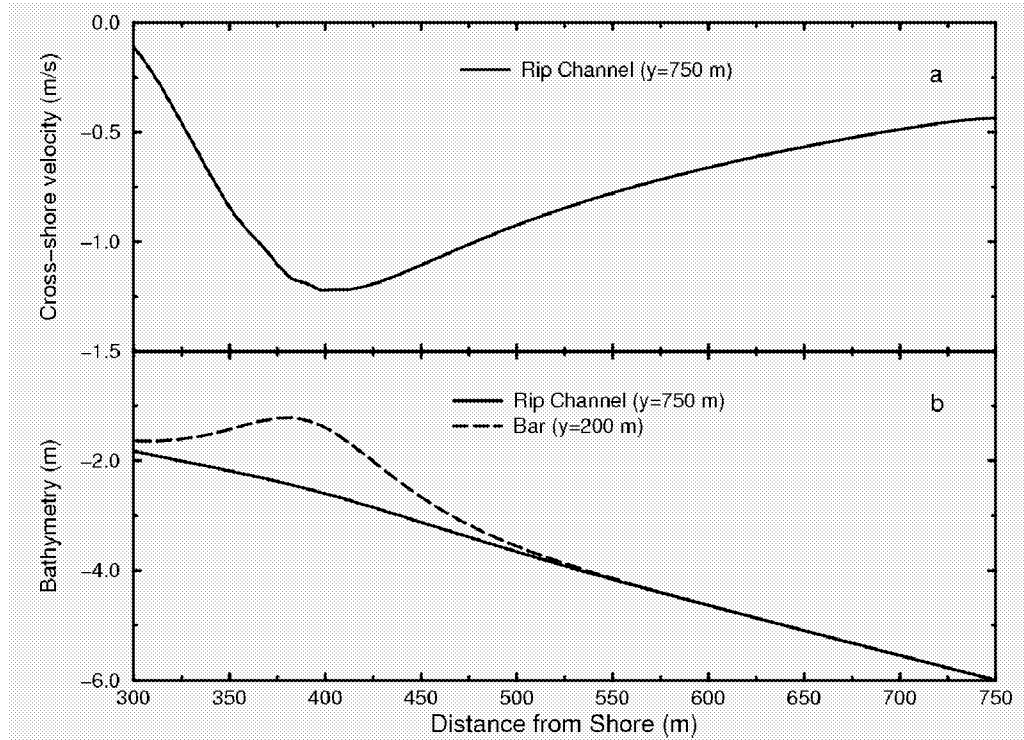


Fig. 8 — Ideal barred beach: (a) A cross-shore transect along the rip channel ($y = 750$ m) of the cross-shore current and (b) cross-shore transects on the bar ($y = 200$ m) and in the rip channel ($y = 750$ m) of the bathymetry.

The strong shear associated with the seaward flowing rip current and shoreward flowing feeder currents presents an opportunity for an unsteady flow to develop. Shearing effects (e.g., vortex formation) become increasingly dominant as lateral mixing and/or frictional dissipation decreases and are much more significant for the rip current than for the alongshore current of the planar beach simply because the magnitude of the shear is larger. The rip current and the oppositely flowing feeder currents are initially similar in magnitude and quite strong (~ 1 m/s), as seen from the alongshore transect at $x = 400$ m in Fig. 5(a). Even at the offshore boundary, the maximum feeder current velocity is still about 25% of the maximum rip current velocity (~ 0.4 m/s). This results in cross-shore velocity profile that is changing quite rapidly in the alongshore direction, creating a region of high shear. In the planar case of BC02 the peak alongshore current was approximately 30 times larger in magnitude than the very weak opposing offshore current, and the offshore tail of the alongshore current was essentially flat. The flat offshore tail of the alongshore current reduced the offshore shear in the ideal planar beach. It is this difference between the circulation patterns of the two beaches that accounts for their different sensitivities to the lateral mixing parameter.

In order to examine unsteady rip current circulation, the lateral mixing coefficient (E_h) is lowered to a value of $0.5 \text{ m}^2/\text{s}$. The value of the nonlinear bottom friction coefficient (C_f) is held fixed at 0.004, the same value used for the steady state condition. The evolution of the rip current circulation is observed over a time period of 31 min, and the initial and final states are shown in Figs. 9(a) and 9(b). As shown by Fig. 9(a), vortices are being generated offshore in the region of high shear between the inward flowing feeder currents and the offshore directed rip current. A vortex initially forms about 500 m offshore and then moves further offshore to the boundary of the domain. It is also apparent from Figs. 9(a) and 9(b) that the fluid motion associated with these offshore vortices affects the overall rip current circulation. The initial vortex circulation of Fig. 9(a) changes the alongshore direction of the rip current, leading eventually to the generation of a similar vortex on the opposite side of the rip current in Fig. 9(b). As a new vortex starts to form, the other vortex recombines with the seaward flow of the rip current. The rip

current moves periodically from one side of the domain to the other in the alongshore direction as this process of vortex generation repeats itself. At the offshore boundary, the rip current typically moves about 150 to 200 m away from the centerline of the channel in either direction. It takes approximately 60 min for the rip current to complete one cycle, moving from one side of the domain to the other and then back again. The period of the rip current oscillation does not change as the lateral mixing is increased from 0.5 to 2.0 m^2/s . Increasing the lateral mixing simply decreases the size of the shear-induced vortices and the excursion of the rip current in the alongshore direction, but the period of the oscillations is not dependent on the lateral mixing.

A longer 1-day simulation was run to see if this periodic motion continues. In addition to its alongshore motion, the rip current was observed curling up to form a vortex on the end of the upper bar at the channel. This vortex lasted approximately 80 min, at which point the rip current uncurled and continued its alongshore motion. This behavior indicates the complexity of the unsteady rip current motion over long periods of time even in the absence of significant bathymetric perturbations and wave-current interaction. Field studies of such vortices have thus far been only qualitative, making a direct comparison to the model results difficult. Chen et al. (1999) and Haas and Svendsen (2000) observe similar vortex-induced motion in their rip current modeling studies as well.

The asymmetric vortex formation evident in Fig. 9 may be the result of perturbations introduced by the slight asymmetry in the length of the bars. Such asymmetries can lead to an unsteady rip current as noted by Chen et al. (1999). To confirm that the unsteady rip current circulation is physical and not simply the manifestation of numerical perturbations, Gaussian noise was added to the radiation stress gradient field. The x and y components of the radiation stress gradient at individual points could deviate by as much as 5% from their original value. The unsteady motion of the rip current was not noticeably affected by the added noise, indicating that it is indeed a robust feature of the rip current circulation.

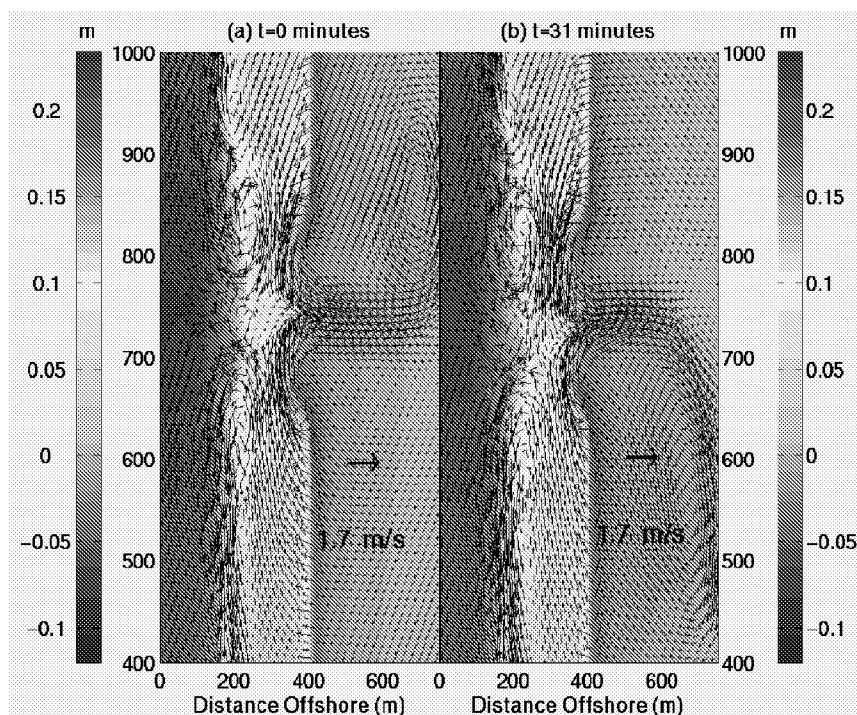


Fig. 9 — Ideal barred beach: Snapshots of the unsteady rip current sea surface elevations and currents at (a) $t = 0$ min and (b) $t = 31$ min. Arrows representing a 1.7- m/s current indicate the magnitudes of the current field vectors. Note: Only every third current vector of the current vector field is plotted.

SIMULATION OF A LABORATORY SCALE RIP CURRENT

In order to validate the ADCIRC rip current simulations, model-data comparisons are made to measurements that were taken during the laboratory rip current experiment of Haller and Dalrymple (1999). This experiment, which was performed in a directional wave basin at the Center for Applied Coastal Research at the University of Delaware, measured wave heights, water levels, and currents on a barred beach with two rip current channels; the bathymetry of the wave basin is depicted in Fig. 10. Further details of the experiment can be found in Haller and Dalrymple (1999). The data of Test B presented in Haller and Dalrymple (1999) is used to validate the results of our simulations. Simulating this laboratory experiment is also an important test of ADCIRC's ability to model wave-driven nearshore flows at very small scales of $O(0.1 \text{ m})$.

The simulation domain represents an 11 by 18.2 m section of the wave basin in which measurements were made (Fig. 10). The rip channels are located at $\frac{1}{4}$ and $\frac{3}{4}$ of the alongshore basin width and both rip channels have alongshore widths of approximately 1.8 m. The Haller and Dalrymple (1999) experiment focused on the rip channel in the upper half of the domain, therefore model-data comparisons are made in this region as well. The laboratory experiment is simulated on a finite element grid with 20,313 computational nodes and a node spacing of 0.1 m. The measured bathymetry, which is resolved to 0.2 m, is interpolated onto the finite element grid. A simulation length of 14.4 h, with a time step of 0.025 s, achieves a converged solution and satisfies the Courant condition. Closed lateral boundaries are used rather than radiation boundary conditions in order to simulate laboratory conditions. A water level of zero is maintained at the offshore boundary and a no-flow boundary is imposed at the shoreline. The REF/DIF1 grid also has a resolution of 0.1 m and the normally incident wave height is 0.048 m with a period of 1.0 s.

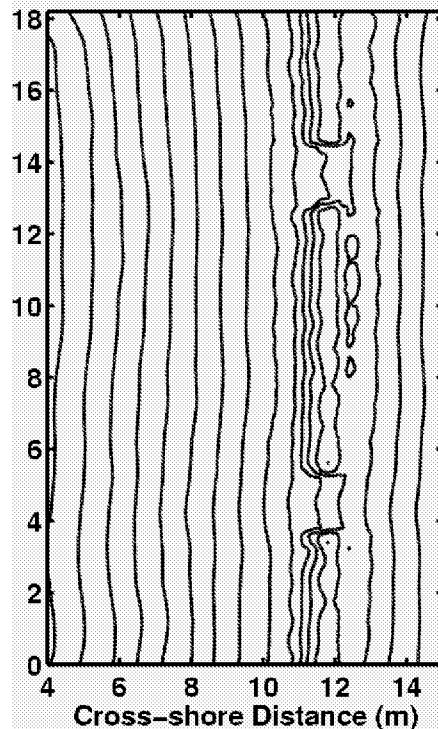


Fig. 10 — Bathymetry of the Haller and Dalrymple (1999) laboratory domain. The bathymetric contour interval is 0.025 m.

Steady State

A parameter study is undertaken to determine the values of E_h and C_f that produce realistic steady state circulation patterns. A steady state circulation pattern that is qualitatively similar to the time-averaged experimental observations is obtained using values of $0.01 \text{ m}^2/\text{s}$ and 0.004 , respectively, for E_h and C_f . It should be pointed out that the value of the lateral mixing coefficient is an order of magnitude smaller than the values used in the ideal barred beach simulations. Because the resolution of the laboratory simulation is an order of magnitude higher than that employed for the ideal barred beach simulation, E_h must also be decreased by an order of magnitude since lateral mixing scales with the grid resolution. Appropriate specification of E_h will avoid unrealistic smoothing of the current field.

The upper rip channel, to which comparisons are made, is located at approximately $y = 13.6 \text{ m}$ in Fig. 10. It should be noted that the peak of the alongshore bar is located at approximately $x = 11.8 \text{ m}$. The wave heights and steady state circulation patterns for the upper rip channel (Fig. 11) are qualitatively similar to the steady state wave heights and circulation patterns of our ideal barred beach (Fig. 2). Shoreward feeder currents exist in the channel at the end of each bar and alongshore feeder currents, on both the seaward and shoreward sides of the bar, are directed toward the rip channel (Fig. 11(b)). Also, clockwise and counterclockwise rotating vortices are generated where alongshore currents converge at the rip channel shoreward of the bar. In contrast, bathymetric irregularities, particularly along the length of the bar, generate wave heights and circulation patterns that are very asymmetrical about the upper rip channel, unlike those seen in the ideal barred beach simulations (Fig. 2).

It should be pointed out that the presence of the lower rip channel does affect the overall circulation within the domain (e.g., circulation patterns shoreward of the bar). The upper rip current is biased towards the center of the domain because the flow at the upper rip channel is asymmetric (Fig. 11(b)) and because of circulation patterns generated by the lower rip channel (not shown). In a similar modeling study of the same laboratory domain, Haas et al. (1998) found that wave-current interaction was necessary to obtain a rip current that had the correct offshore strength and direction. The ADCIRC simulation produces a rip current biased towards the center of the basin, but the rip current in Fig. 11(b) is more intense and extends further offshore than the observed rip current (Haas et al. 1998). This strongly suggests that wave-current interaction is necessary to reproduce the observed mean circulation.

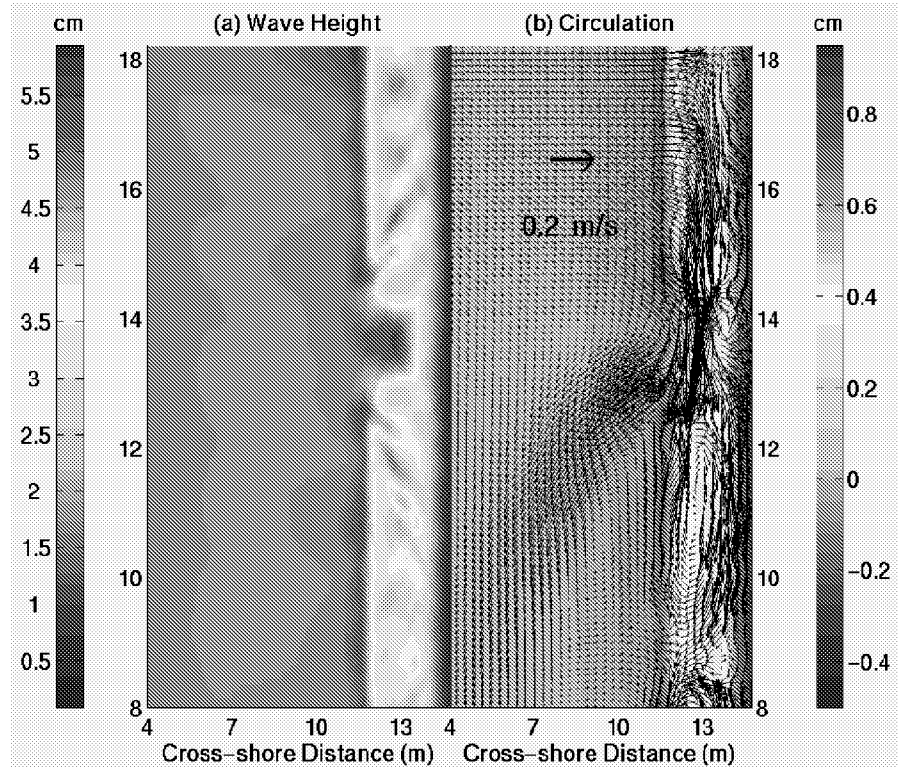


Fig. 11 — Laboratory domain: (a) REF/DIF1 solution for the wave height field and (b) ADCIRC solution for the steady state water levels and currents. An arrow representing a 0.2 m/s current indicates the magnitudes of the current field vectors. Note: Only every third current vector of the current vector field is plotted.

Model results are compared to the time-averaged mean observations along the same x and y transects that were used in Haller and Dalrymple (1999). The wave height and steady state water level along cross-shore transects on the bar ($y = 9.2$ m) and in the rip channel ($y = 13.6$ m) are in good agreement with the results of Haller and Dalrymple (1999) (Figs. 12(a) and 12(b)); Fig. 12(c) provides a bathymetric reference for Figs. 12(a) and 12(b). The depth-limited monochromatic wave breaking of REF/DIF1 results in predicted wave heights with sharper peaks than the observed wave heights on the bar and in the rip channel (Fig. 12(a)). Differences between the predicted and observed set-up and set-down (Fig. 12(b)) are in part a result of the simple depth-induced wave breaking mechanism used by REF/DIF1. Additional discrepancies exist between the ADCIRC results and the experimental data, most likely a result of neglecting wave-current interaction. Wave-current interaction is probably significant in the rip channel, causing the observed waves to break earlier than the predicted ones (Fig. 12(a)). In addition, the no-flow shoreline boundary results in a slightly greater water level near the shoreline than would be expected on a real planar-like beach. This might account for the discrepancy between the model and the data in Fig. 12(b) around $x = 13.5$ m.

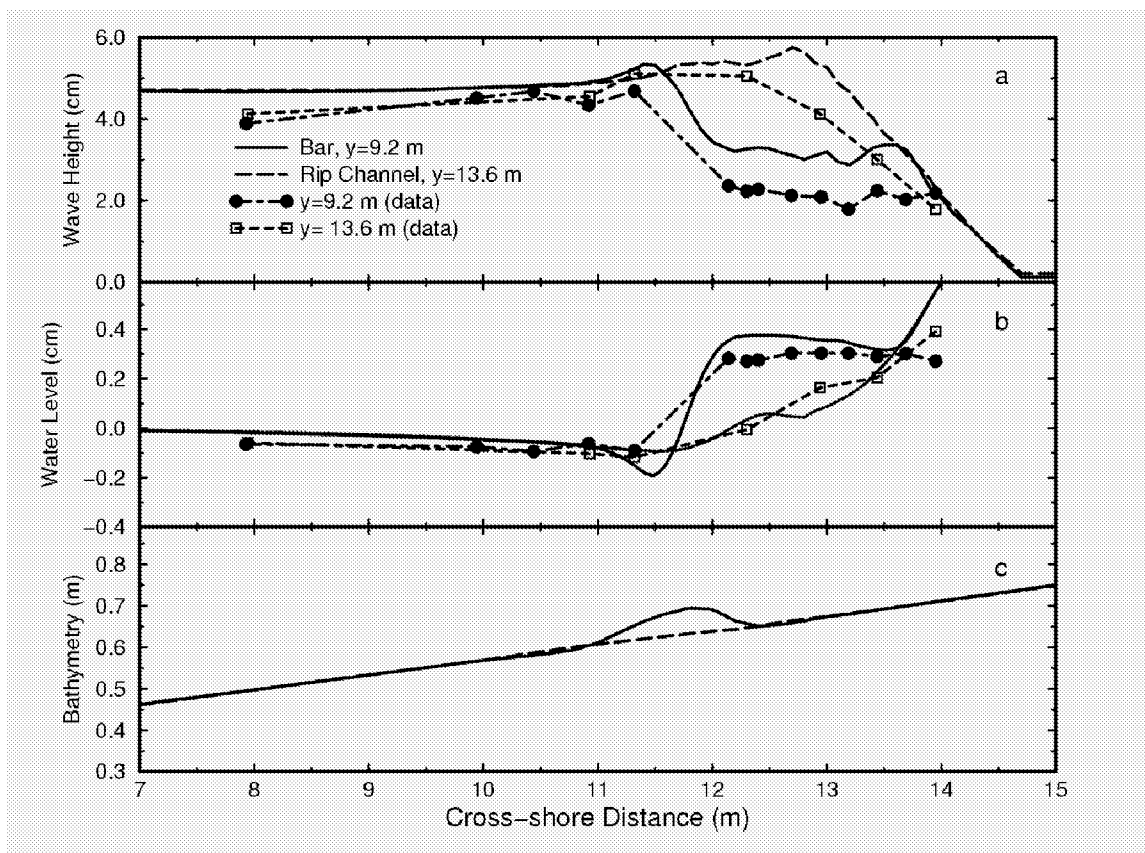


Fig. 12 — Laboratory domain: Model-data comparisons are made (a) between the REF/DIF1 wave heights and the measured mean wave heights and (b) between the steady state ADCIRC solution for the water level and the measured mean water level. (c) Transsects of the bathymetry on the bar ($y = 9.2$ m) and in the rip channel ($y = 13.6$ m).

In Fig. 13, a comparison is made to the measured time-averaged alongshore current along cross-shore transects at $y = 9.2$ m and $y = 11.2$ m. The ADCIRC alongshore current profiles in Fig. 13 have the same qualitative trends as the observations, although the model results appear to be shifted offshore. The transect for $y = 11.2$ m, aside from the difference in the position of the peak, has about the same maximum and minimum values as the data and a similar peak width. The peak in the $y = 11.2$ m alongshore current corresponds to the feeder current on the bar, just below the rip channel. The transect along $y = 9.2$ m has a peak that is closer to the position of the observed peak, but the seaward trend of the transect significantly overpredicts the alongshore velocity. Because the predicted rip current turns more gradually towards the center of the basin than the observed rip current, the predicted alongshore current transect at $y = 11.2$ m (Fig. 13) has a minimum that is further offshore than the observed alongshore current. Haas et al. (1998) observed that the time-averaged rip current direction was strongly biased towards the center of the domain and that the shoreward recirculation cells became smaller, not extending as far offshore, when wave-current interaction was included in their model. This change in the recirculation cells due to wave-current interaction would account for the difference in the observed and predicted peaks along $y = 11.2$ m. The Haas et al. (1998) observation also suggests that the predicted offshore ($x < 11.5$ m) alongshore current at $y = 9.2$ m in Fig. 13 is less negative than the observed alongshore current because the predicted rip current does not turn sharply enough.

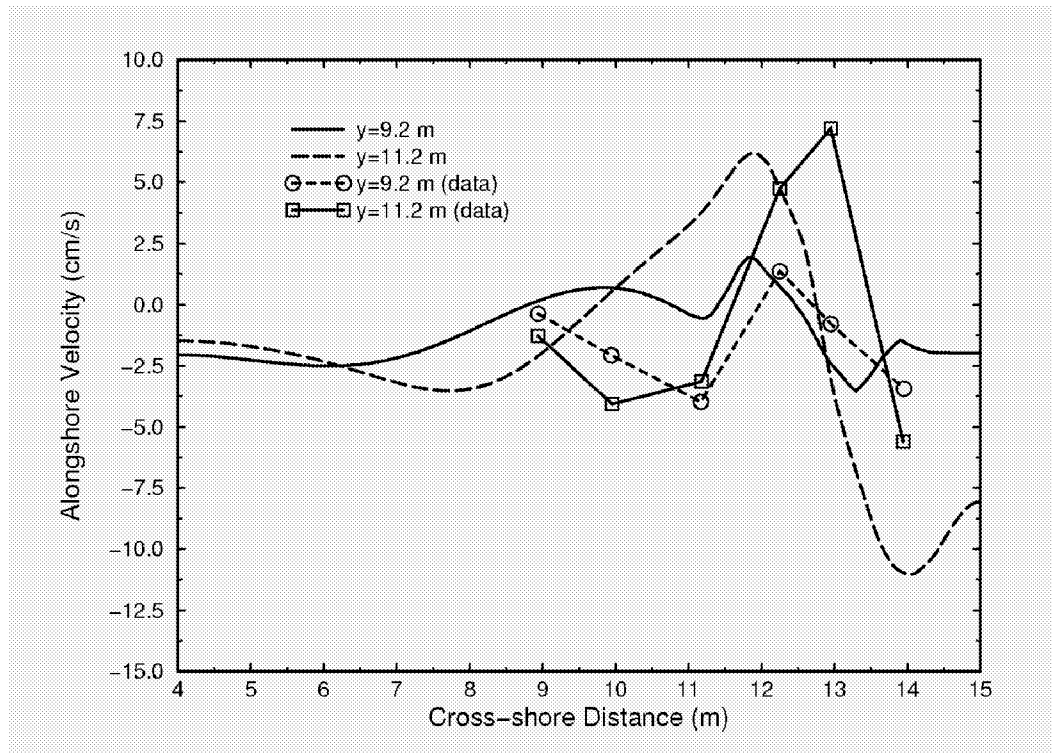


Fig. 13 — Laboratory domain: Model-data comparisons are made between the ADCIRC steady state solution for the alongshore current and the measured mean alongshore current using cross-shore transects at $y = 9.2$ m and $y = 11.2$ m.

The ADCIRC alongshore and cross-shore currents, shown respectively in Figs. 14 and 15 along transects at $x = 11.5$ m, 11.8 m, and 12.0 m in the alongshore direction, are compared to time-averaged observations along the same transects between $y = 13$ m and $y = 14.5$ m. Note that the laboratory data is at the mouth of the upper rip channel, where the rip current emerges. The ADCIRC alongshore currents of Fig. 14 have the correct trends but differ significantly from the observations in their magnitudes. The magnitudes of the ADCIRC cross-shore currents in Fig. 15 are in good agreement with the data, although the ADCIRC results appear to be shifted relative to the observations by approximately 0.5 m. The differences between the predicted and observed currents indicate that the predicted rip current direction differs from the observed rip current direction by about 0.5 m in its alongshore position. This difference might also account for the slight discrepancies between the relative strengths of the predicted and observed cross-shore currents (Fig. 15). It should be pointed out that the observed rip current moves back and forth in the alongshore direction (Haller et al. 1997) and that comparisons are being made to the time-averaged experimental observations. Because the ADCIRC simulation represents a steady state, it will not necessarily reproduce all of the time-averaged characteristics of the observed rip current. In addition, it is not known what effect wave-current interaction has on the direction of the observed mean rip current in this region of the upper rip channel.

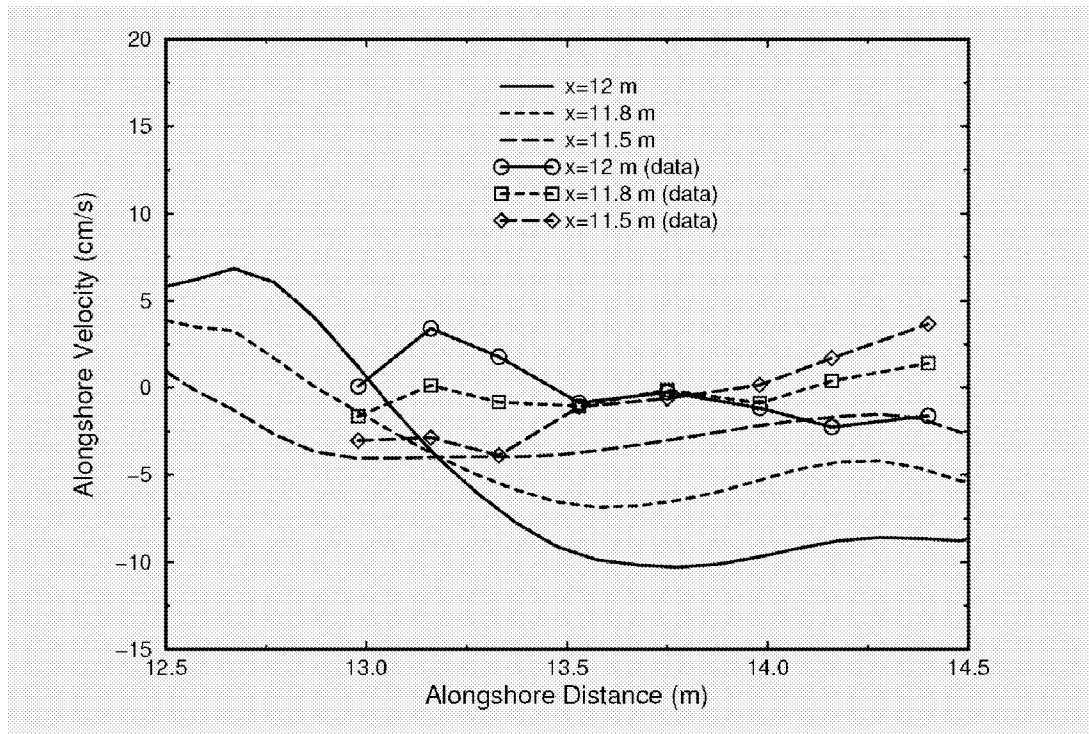


Fig. 14 — Laboratory domain: Model-data comparisons are made between the ADCIRC steady state solution for the alongshore current and the measured mean alongshore current using alongshore transects at $x = 11.5$ m, $x = 11.8$ m, and $x = 12$ m.

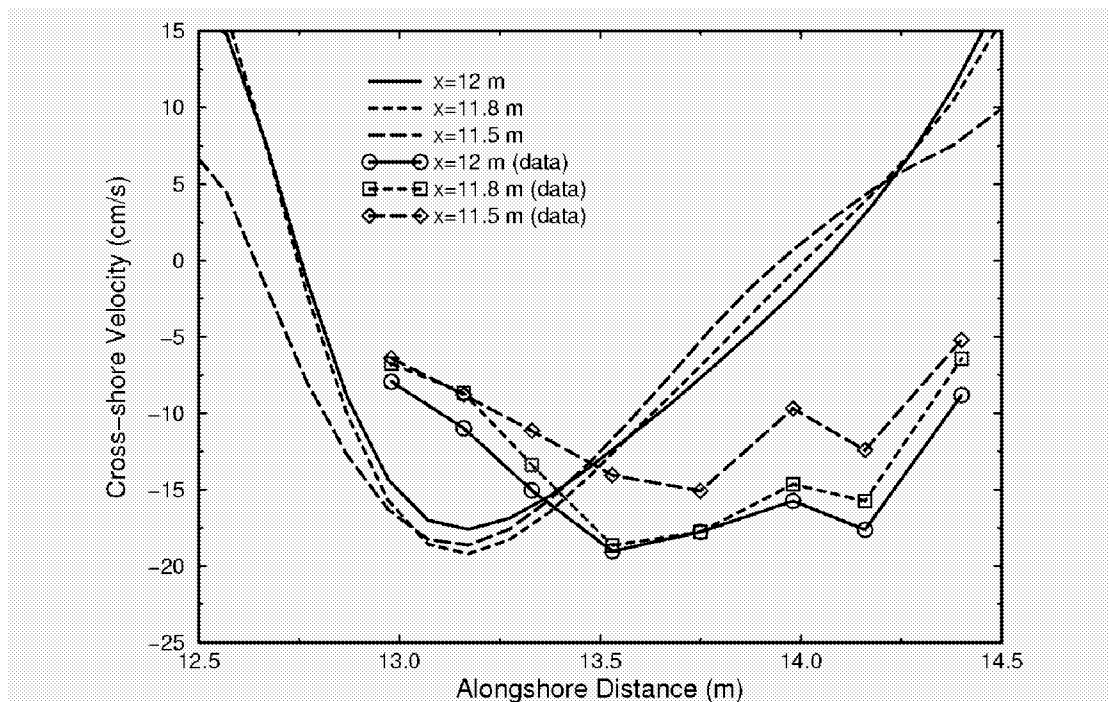


Fig. 15 — Laboratory domain: Model-data comparisons are made between the ADCIRC steady state solution for the cross-shore current and the measured mean cross-shore current using alongshore transects at $x = 11.5$ m, $x = 11.8$ m, and $x = 12$ m.

Unsteady State

The rip current observed by Haller and Dalrymple (1999) exhibited unsteady behavior throughout their experiment. Values of E_h and C_f that produce a realistic unsteady rip current are determined to be, respectively, $0.005 \text{ m}^2/\text{s}$ and 0.004 . It should be pointed out that the shear-induced vortex formation observed in the ideal barred beach simulations does not occur in any of the unsteady laboratory simulations. Lowering the lateral mixing below $0.005 \text{ m}^2/\text{s}$ or the nonlinear friction coefficient below 0.002 results in a computationally unstable solution, suggesting that greater nodal resolution and subsequently smaller values of E_h are necessary to observe shear-induced vortices at the spatial scales of this laboratory experiment.

When the rip current becomes unsteady, it moves in a periodic manner back and forth in the alongshore direction. The initial and final circulation patterns of the rip current are shown for a time period of 45 s in Figs. 16(a) and 16(b). This periodic motion propagates along the length of the rip current in a wave-like manner, changing the direction of the rip current. Note that the large vortex centered below the rip current at $(x = 9.4 \text{ m}, y = 10.4 \text{ m})$ is a stable feature of the unsteady circulation. The periodic motion of the rip current can also be characterized through vorticity transport. The vorticity patterns of the initial and final rip current, displayed in Fig. 17, correspond to the circulation seen in Fig. 16. Pairs of opposite vorticity move along the rip current and dissipate as they reach the middle of the domain (Fig. 17). Chen et al. (1999) also observe vorticity transport along the rip current in their modeling study of the Haller experiment. A time series of the alongshore current is plotted for two points along the rip current in Fig. 18. The two points are located along a cross-shore transect at $y = 13.5 \text{ m}$ with offshore positions at $x = 9.16 \text{ m}$ and 10.1 m . The wave-like motion of the rip current is apparent from the periodic oscillations of the alongshore current as well as the phase lag between the alongshore current values at the two points. Both time series of the alongshore current indicate that the motion of the rip current has a period of approximately 130 s.

The unsteady rip current observed by Haller et al. (1997) was reported to have two distinct time scales of unsteady motion: 1) a long period motion of about 140 s correlated with the alongshore migration of the rip current and 2) a short period motion of about 17 s correlated with jetlike vortex generation. Figure 18 depicts a long-period unsteady motion of about 130 s for the simulated rip current; however, unsteady rip current motion with a period of about 17 s is not evident. Current velocities were output during the simulation every 3 s in order to resolve the 17 s short period motion (if it was present). Because the short period motion is associated with shear-induced vortices (Haller et al. 1997; Chen et al. 1999) (which do not occur in this simulation), a higher grid resolution and a subsequently lower lateral mixing coefficient, as previously discussed, are likely necessary to resolve such features. The computational effort to simulate this domain with greater grid resolution makes such an investigation prohibitive at this time. Although the solution for the long period unsteady motion and the unsteady rip current motion observed in the ideal barred beach do indicate that a realistic solution for the unsteady laboratory rip current can be obtained using ADCIRC.

Wave-current Interaction

It has been accepted for some time that wave-current (w-c) interaction plays an important role in the dynamics of rip currents (Dalrymple 1978). The offshore flow of the rip current interacts strongly with the incident waves that create it, causing the waves to refract, shoal, and break. This can create large radiation stress gradients that oppose the rip current and change its direction. A change in the rip current direction will result in a change in the wave field as well, creating a feedback mechanism between the waves and currents. Unfortunately it is quite difficult to determine the affects of w-c interaction on actual rip currents (Smith and Largier 1995).

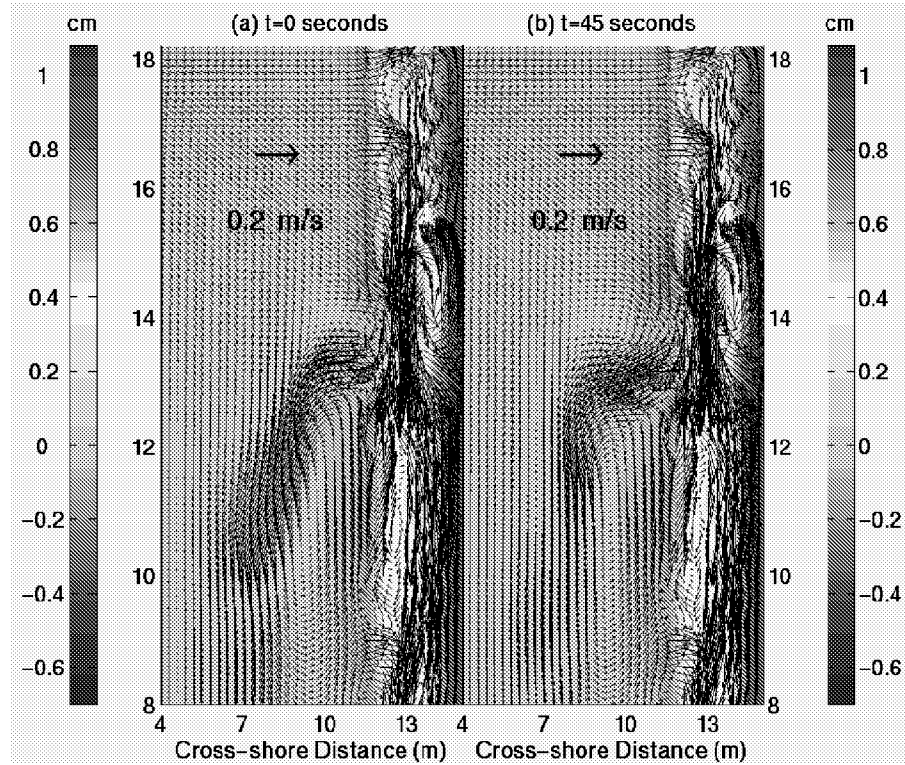


Fig. 16 — Laboratory domain: Snapshots of the ADCIRC water levels and currents for the unsteady rip current at (a) $t = 0$ s and (b) $t = 45$ s. Arrows representing a 0.2 m/s current indicate the magnitudes of the current field vectors. Note: Only every third current vector of the current vector field is plotted.

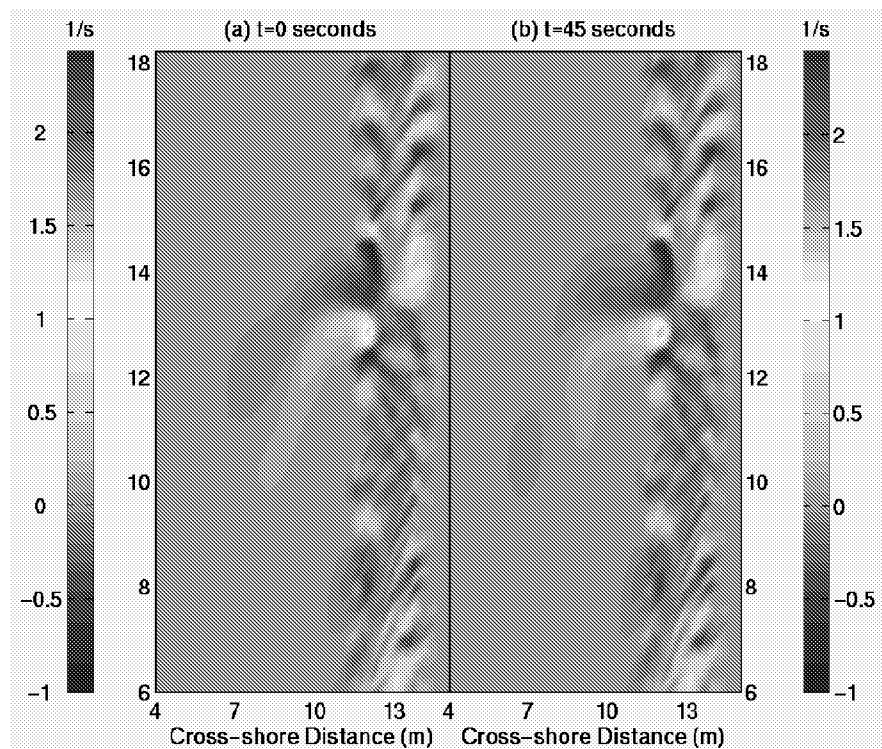


Fig. 17 — Laboratory domain: Snapshots of the unsteady rip current vorticity (determined from the ADCIRC solution for the velocity) at (a) $t = 0$ s and (b) $t = 45$ s.

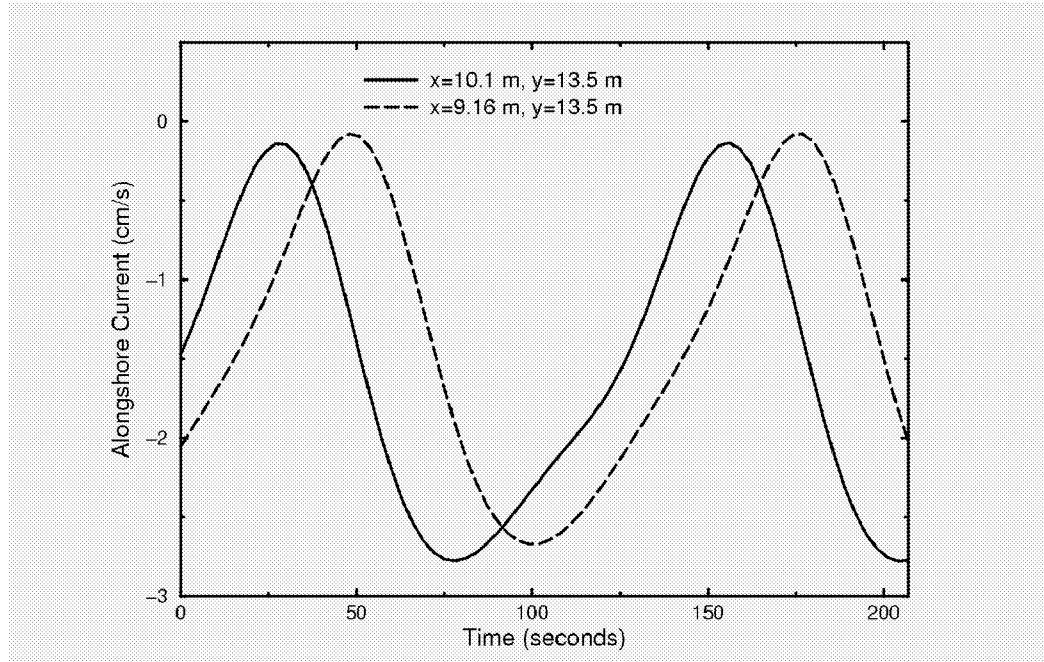


Fig. 18 — Laboratory domain: ADCIRC solution for the unsteady alongshore current along a cross-shore transect in the rip channel ($y = 13.5$ m). The values of the alongshore current at two different points ($x = 9.16$ m and $x = 10.1$ m) along the cross-shore transect are shown for a time interval of 207 s. Note that the value of x is decreasing in the offshore direction.

The effects of w-c interaction on the unsteady circulation of the ideal barred beach are examined here by iteratively coupling ADCIRC with REF/DIF1. The previously discussed unsteady case with $E_h = 0.5$ m^2/s and $C_f = 0.004$ is used because both vortex formation and w-c interaction are present in actual rip currents. In addition, the ideal barred beach does not have bathymetric perturbations that would add further complexity to the circulation and therefore make it more difficult to discern the effects of w-c interaction. There are several issues to be addressed in coupling these models, the two most important being the time period between each iterative coupling and modeling the effect of the currents on the waves (e.g., wave breaking due to strong opposing currents). No attempt is made to thoroughly address these issues in this initial study. Instead, only the qualitative changes that occur in the unsteady rip current of the ideal barred beach, as a result of the inclusion of w-c interaction, are examined.

First, the ADCIRC circulation model is run for an initial spin-up period, as was done in the previous simulations, until a stable converged solution is obtained. During this initial spin-up period, the wave field is held constant. The coupling of ADCIRC and REF/DIF1 is accomplished by using the elevation and current fields produced by ADCIRC to modify the REF/DIF1 wave field. ADCIRC is then run forward for an appropriately small, predetermined time interval (the iteration interval), forced by a new wave field. The duration of the iteration interval is based on the response of the circulation to a new wave-forcing field. The circulation should not change during the iteration interval to the extent that the wave-forcing field (assuming w-c interaction) is completely uncorrelated with it. At the end of this iteration interval, the wave field is recalculated and the process is repeated until the end of the simulation period is reached. For the particular case presented here, an iteration interval of 8.64 s was determined to be small enough to allow for realistic w-c interaction. The coupled simulation extends for a total time of only 86.4 s or 10 iterations. The vortex-induced motion of the unsteady rip current, with a period of approximately 60 min, cannot be observed on this time scale. Longer simulations will be possible in the future upon implementation of the MPI parallel version of ADCIRC-2DDI.

It should be noted that the current field is not smoothed in any way before being input to REF/DIF1. Because REF/DIF1 is a parabolic wave model, it does not allow for the backward propagation of waves. Circulation features, such as small intense eddies in the current field, can lead to the backward propagation of waves through refraction, causing REF/DIF1 to terminate its calculation. The development of circulation patterns that cause the backward propagation of waves prevent long iteration intervals as well as lengthy total simulation times. In order to perform longer w-c interaction simulations of nearshore flow, either an approach must be developed to smooth the current field or a different wave model must be applied to the problem. Either approach is beyond the scope of this initial w-c interaction study.

The initial wave height and circulation fields, following the spin-up period, are shown in Fig. 19. The REF/DIF1 wave field for the first iteration (Fig. 20(a)) is modified using this circulation field (Fig. 19(b)) as input. Following the first iteration, w-c interaction causes the incident waves to refract, shoal, and break in the rip channel as seen from the wave heights of Fig. 20(a). The maximum wave height in Fig. 20(a), located seaward of the rip channel, is almost twice that of the maximum wave height in Fig. 19(a). Because of refraction due to the rip current, a region where the wave direction is very large relative to the direction of the rip current is created. This narrow region is located between the large wave heights seaward of the rip channel in Fig. 20(a). Because the waves are almost perpendicular to the current, they do not shoal significantly. All of these modifications to the wave field result in strong radiation stress gradients that subsequently change the rip current circulation near the mouth of the rip channel (Fig. 20(b)). The rip current velocities in Fig. 20(b) are large where the opposing radiation stress gradients are small, creating a narrow region at the mouth of the rip channel where the rip current is very intense. The rip current is more intense in the same regions where the wave direction is almost perpendicular to its direction.

Following the tenth iteration, the wave heights (Fig. 21(a)) are similar to those of the first iteration (Fig. 20(a)), but more fine structures are present due to the greater complexity of the current field from the ninth iteration (not shown). Near the mouth of the rip channel the resulting circulation at the tenth iteration (Fig. 21(b)) is much more complex than the circulation of the first iteration (Fig. 20(b)) due to the modified wave field (Fig. 21(a)). It is interesting to note how quickly the circulation responds to the updated wave forcing. The entire coupled simulation is only about 1.5 min, but within that short time period the circulation changes dramatically at the mouth of the rip channel and throughout the entire region shoreward of the bar (Fig. 21(b)). Because the simulation does not reach a converged steady state, it is continually evolving in response to the updated wave field, thus the changes observed in the circulation are due in part to the new wave field as well as the time-dependent circulation from the previous iteration.

It is difficult to measure unsteady rip currents in the field because of their spatial extent and complex variations in space and time. Field studies typically present only the time-averaged rip current pattern. The deployment of pressure sensors and current meters for such nearshore measurements can also be quite challenging. Although new techniques have been developed for studying rip currents (Smith and Largier 1995), more work needs to be done. The lack of observations makes it impossible to verify how realistic these w-c interaction rip current solutions are for the ideal colinear beach and the extent to which shear-induced vortices and w-c interaction contribute individually to the unsteady motion of actual rip currents is still an open question. Overall, more observational data are needed to understand the unsteady behavior of rip currents and to validate the results of fully coupled modeling studies.

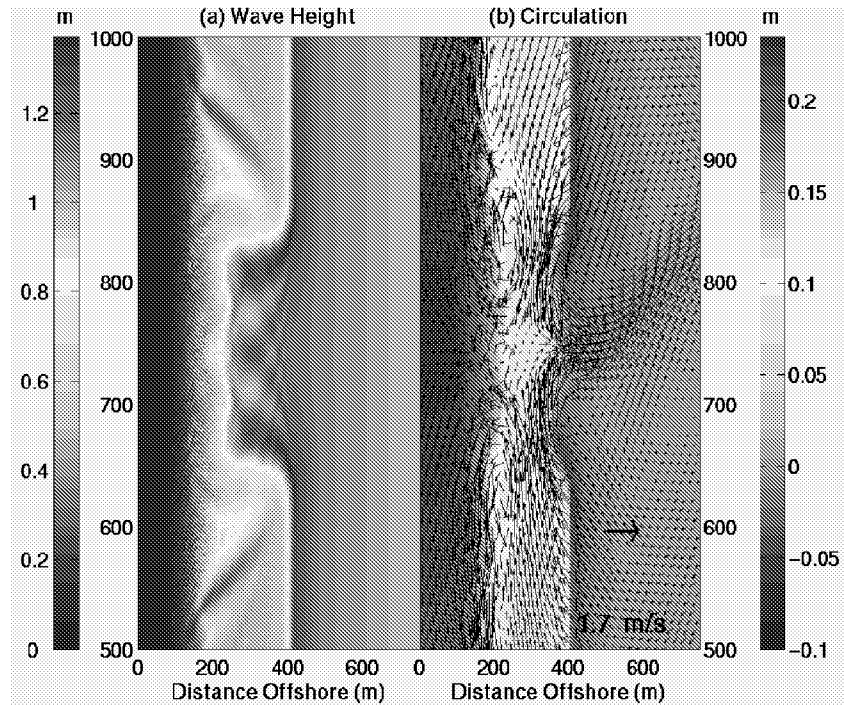


Fig. 19 — Ideal barred beach: (a) Initial REF/DIF1 solution for the wave heights. (b) Initial ADCIRC solution for the sea surface elevations and the currents. An arrow representing a 1.7 m/s current indicates the magnitudes of the current field vectors. Note: Only every third current vector of the current vector field is plotted.

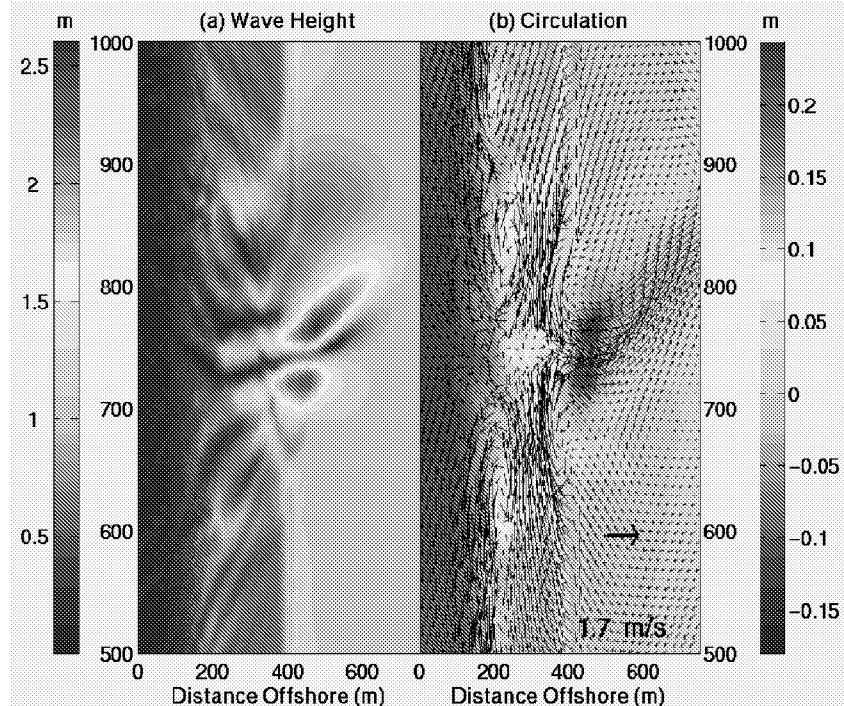


Fig. 20 — Ideal barred beach. Coupled model after iteration 1: (a) REF/DIF1 wave heights used to force the ADCIRC circulation. (b) ADCIRC sea surface elevations and currents. The wave field in (a) incorporates the effects of the initial sea surface elevations and currents seen in Fig. 19(b). An arrow representing a 1.7 m/s-current indicates the magnitudes of the current field vectors. Note: Only every third current vector of the current vector field is plotted.

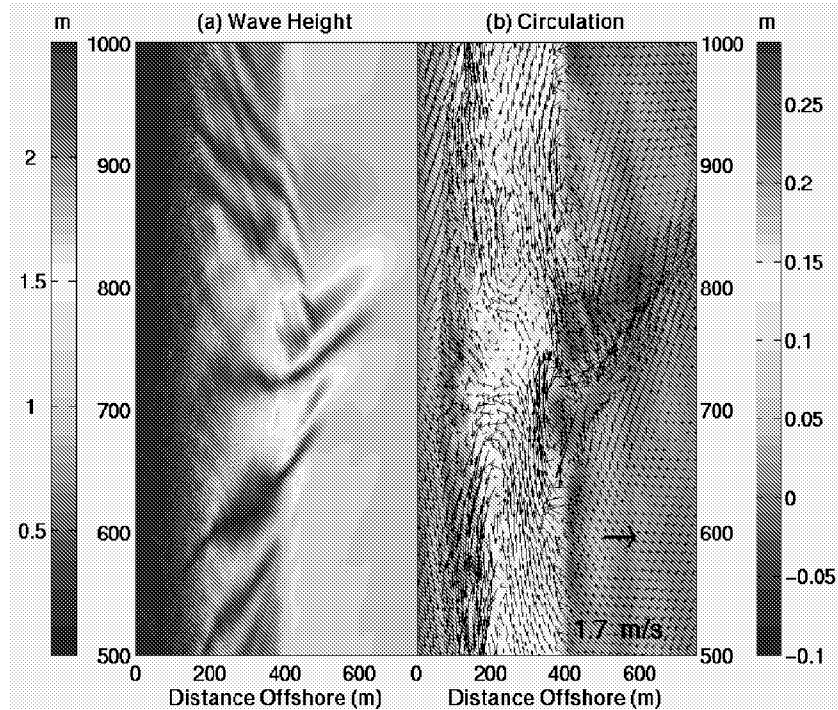


Fig. 21 — Ideal barred beach. Coupled model after iteration 10: (a) REF/DIF1 wave heights used to force the ADCIRC circulation. (b) ADCIRC solution for the sea surface elevations and currents. The wave field in (a) incorporates the effects of the sea surface elevations and currents from the ninth iteration (not shown). An arrow representing a 1.7 m/s current indicates the magnitudes of the current field vectors. Note: Only every third current vector of the current vector field is plotted.

CONCLUSION

In this second study of wave-induced nearshore circulation, rip currents on barred planar beaches were simulated using the ADCIRC-2DDI and the REF/DIF1 wave models. Although rip currents play an important role in the sediment transport of beaches and are a significant hazard to swimmers, many of their characteristics (e.g., shear-induced vortices) are still not well understood. The dual purpose of this study was to apply the ADCIRC-2DDI model to the problem of simulating complex wave-induced nearshore circulation and to better understand the characteristics of rip currents.

In order to better understand the qualitative aspects of large scale rip currents, an ideal planar beach approximately 1 km² in area, with an alongshore bar and a single rip channel, was simulated. The steady and unsteady solutions for the circulation were investigated by examining the relative influence of the lateral mixing and nonlinear bottom stress. Good qualitative agreement was found between these results and time-averaged characteristics of rip currents observed in field studies. In addition, the contributions of wave-induced set-up/set-down, pressure gradients, and inertial forces to the current field in the rip channel were determined. The unsteady circulation of the ideal barred beach was examined as well by reducing the lateral mixing. Shear-induced vortices, generated by the rip current flow, redirected the rip current circulation, causing it to move periodically back and forth in the alongshore direction. In addition, longer simulations revealed that the rip current could also exhibit significant cross-shore motion. This unsteady behavior was qualitatively quite similar to rip current behavior observed in field studies. Unfortunately, there are very few quantitative measurements of the space and time varying characteristics of actual unsteady rip currents that can be used to validate these results.

Model-data comparisons were made to the laboratory rip current experiments of Haller and Dalrymple (1999). The data from Test B of this experiment was used to make direct comparisons to the ADCIRC-2DDI steady state solution for the water level and the current. Good agreement was found between the predicted water levels and the observed values. The primary differences between the ADCIRC results and the data can be accounted for in terms of the wave model's depth-limited wave breaking criterion and the absence of w-c interaction in the simulation. Fairly good agreement was found between the predicted and measured alongshore and cross-shore current, although some significant discrepancies existed as well. In all the cases examined, the positions of the predicted alongshore and cross-shore currents were shifted relative to the observations in either the alongshore or the cross-shore direction. The differences between the model results and the data strongly suggest that w-c interaction is required to obtain a better solution using the ADCIRC model.

An unsteady solution for the laboratory rip current was obtained for comparison with the observed unsteady rip current in the Haller and Dalrymple (1999) experiment by reducing influence of lateral mixing. The unsteady solution for the rip current reproduced the observed long period motion of approximately 140 s but failed to reproduce the short period motion of approximately 17 s. Because the short period motion is associated with shear-induced vortices, this result suggests that a lower value of the lateral mixing coefficient is required to reproduce the short period oscillations. The lateral mixing in ADCIRC scales with the grid resolution and, in this case a finer computational grid, is required to lower the lateral mixing further. This issue was not resolved due to the computational effort that would have been involved in examining the Haller and Dalrymple (1999) domain at significantly higher grid resolutions.

In the last section of this report, w-c interaction was investigated by coupling the ADCIRC-2DDI model with the REF/DIF1 wave model. The respective ADCIRC and REF/DIF1 solutions for the unsteady circulation and the wave field on the ideal barred beach were noticeably altered by w-c interaction. The waves refracted, shoaled, and broke further offshore than in the original simulation, resulting in a significantly modified radiation stress gradient field. The modified forcing field, in turn, altered the offshore flow of the rip current. In particular, the offshore flow of the rip current became divided into regions of strong and weak offshore flow. This corresponded directly to the modified structure of the wave field. A more detailed analysis of the wave and circulation fields from these simulations is beyond the scope of this report. Because there have not been any field studies that measure w-c interaction quantitatively, it is impossible to validate these results and determine the role played by w-c interaction in the motion of unsteady rip currents.

This study and the results of BC02 demonstrate that the ADCIRC-2DDI model is capable of simulating wave-induced nearshore flow at resolutions ranging from 7.5 m to 0.1 m. This is relevant to coastal modeling studies that require nearshore flows over several different length scales ranging from several kilometers to several meters. Because ADCIRC now has the capability of simulating wave-induced forcing in addition to tidal and wind forcing, it can be applied to a broad range of coastal problems such as wave-driven flow in tidal inlets. Future studies of wave-induced circulation will employ different wave models, such as SWAN (Booij et al. 1999), and will examine the sensitivities of the circulation to the wave model formulation (e.g., multispectral waves, phase-resolving).

ACKNOWLEDGMENTS

The authors would like to thank Dr. Merrick Haller at the Department of Civil, Construction, and Environmental Engineering, Oregon State University and Dr. Robert Dalrymple and Dr. Kevin Haas at the Center for Applied Coastal Research, University of Delaware for the use of their rip current and bathymetry data. Special thanks are extended to Dr. James Kaihatu and Mr. Erick Rogers, both at the Naval Research Laboratory, for their involvement in preliminary work and ongoing discussions with regard to nearshore modeling. The authors would also like to thank Dr. Qin Chen at the University of

South Alabama, Dr. Donald Slinn at the University of Florida, Gainesville, and Dr. Jayaram Veeramony at Mississippi State University for insightful discussions regarding this work. Special thanks to Ms. Catherine Edwards of the Naval Research Laboratory for assistance in creating some of the figures. This research is supported by the Office of Naval Research through the Naval Research Laboratory, BE-35-2-64 and BE-35-2-73.

REFERENCES

Blain, C.A., J.J. Westerink, and R.A. Luetlich, 1994. The Influence of Domain Size on the Response Characteristics of a Hurricane Storm Surge Model, *J. Geophys. Res.* **99**, C9, 18467-18479.

Blain, C.A., J.J. Westerink, and R.A. Luetlich, 1998. Grid Convergence Studies on the Prediction of Hurricane Storm Surge, *Int. J. Num. Methods Fluids* **26**, 369-401.

Blain, C.A., and M. Cobb, 2002. Application of a Shelf-Scale Model to Wave-Induced Circulation: Alongshore Currents on Plane and Barred Beaches, submitted to the *J. Atmos. Oceanic Technol.*

Booij, N., R.C. Ris, and L.H. Holthuijsen, 1999. A Third-Generation Wave Model for Coastal Regions, Part 1, Model Description and Validation, *J. Geophys. Res.* **104**(C4), 7649-7666.

Bowen, A.J., 1969. Rip Currents 1. Theoretical Investigations, *J. Geophys. Res.* **73**, 5467-5478.

Chen, Q., R.A. Dalrymple, J.T. Kirby, A.B. Kennedy, and M.C. Haller, 1999. Boussinesq Modeling of a Rip Current System, *J. Geophys. Res.* **104**(C9), 20,617-20,637.

Dalrymple, R.A., 1975. A Mechanism for Rip Current Generation on an Open Coast, *J. Geophys. Res.* **80**, 3485-3487.

Dalrymple, R.A., 1978. Rip Currents and Their Causes, *Proc. 16th Intl. Conf. Coast. Engrg., Vol. 2*, Hamburg, Germany, ASCE, 1414-1427.

Drønen, N., H. Karunarathna, J. Fredsøe, B.M. Sumer, and R. Deigaard, 1999. The Circulation over a Longshore Bar with Rip Channels, *Coastal Sediments '99: Proceedings of the 4th International Symposium on Coastal Engineering and Science of Coastal Sediment Processes*, Reston, VA, ASCE, 577-587.

Haller, M.C., R.A. Dalrymple, and I.A. Svendsen, 1997. Experimental Modeling of a Rip Current System, *Proceedings of WAVES'97*, Virginia Beach, VA, ASCE, 750-764.

Haller, M.C., and R.A. Dalrymple, 1999. Rip Current Dynamics and Nearshore Circulation, Res. Report CACR-99-05, Center for Applied Coastal Research, Univ. of Delaware.

Hamm, L., 1992. Direction Nearshore Wave Propagation Over a Rip Channel: An Experiment, *Proc. of the 23rd Intl. Conf. Coast. Engrg.*, 226-239.

Haas, K.A., I.A. Svendsen, and M.C. Haller, 1998. Numerical Modeling of Nearshore Circulation on a Barred Beach with Rip Channels, *Proc. 26th Coastal Engineering Conference, Vol. 1*, Reston, VA, ASCE, 801-814.

Haas, K.A., and I.A. Svendsen, 2000. Three-Dimensional Modeling of Rip Current Systems, Res. Report CACR-00-06, Center for Applied Coastal Research, Univ. of Delaware.

- Joshi, P.B., 1982. Hydromechanics of Tidal Jets, *J. Waterways, Port, Coast. Ocean Engng.* **108**, WW3, 239-253.
- Kirby, J.T., 1986. Higher-order Approximations in the Parabolic Equation Method for Water Waves, *J. Geophys. Res.* **91**, 933-952.
- Kirby, J.T., and R.A. Dalrymple, 1994. Combined Refraction/ Diffraction Model REF/DIF1, Version 2.5: Documentation and User's Manual, Res. Report CACR-94-22, Center for Applied Coastal Research, Univ. of Delaware.
- Kolar, R.L., and W.G. Gray, 1990. Shallow Water Modeling in Small Water Bodies, *Proc. 8th Int. Conf. Comp. Meth. Water Res.*, Springer-Verlag, Berlin, 149-155.
- Kolar, R.L., J.J. Westerink, M.E. Cantekin, and C.A. Blain, 1994. Aspects of Nonlinear Simulations Using Shallow Water Models Based on the Wave Continuity Equation, *Computers and Fluids* **23**, 523-538.
- LeBlond, P.H., and C.L. Tang, 1974. On Energy Coupling Between Waves and Rip Currents, *J. Geophys. Res.* **79**, 811-816.
- Longuet-Higgins, M.S., and R.W. Stewart, 1964. Radiation Stresses in Water Waves; A Physical Discussion, with Applications, *Deep Sea Research* **11**, 529-562.
- Luetlich, R.A., J.J. Westerink, and N.W. Scheffner, 1992. ADCIRC: An Advanced Three-Dimensional Circulation Model for Shelves, Coasts, and Estuaries, Report 1: Theory and Methodology of ADCIRC-2DDI and ADCIRC-3DL, Technical Report DRP-92-6, U.S. Army Corps of Engineers Waterways Experimental Station, Vicksburg, MS 137 pp.
- McKenzie, P., 1958. Rip-Current Systems, *J. Geol.* **66**, 103-113.
- Özkan-Haller, H.T., and J.T. Kirby, 1999. Nonlinear Evolution of Shear Instabilities, *J. Geophys. Res.* **104**(C11), 25,953-25,984.
- Shepard, F.P., K.O. Emery, and E.C. La Fond, 1941. Rip Currents: a Process of Geological Importance, *J. Geol.* **49**, 337-369.
- Shepard, F.P., and D.L. Inman, 1950. Nearshore Water Circulation Related to Bottom Topography and Wave Refraction, *Trans. Am. Geophys. Union* **31**, 196-212.
- Slinn, D.N., J.S. Allen, P.A. Newberger, and R.A. Holman, 1998. Nonlinear Shear Instabilities of Alongshore Currents over Barred Beaches, *J. Geophys. Res.* **103** (C9), 18,357-18,379.
- Smith, J.A., and J.L. Largier, 1995. Observations of Nearshore Circulation: Rip Currents, *J. Geophys. Res.* **100**(C6), 10,967-10,975.
- Sonu, C.J., 1972. Field Observation of Nearshore Circulation and Meandering Currents, *J. Geophys. Res.* **77**, 3232-3247.
- Van Dongeren, A.R., and I.A. Svendsen, 2000. Nonlinear and 3D Effects in Leaky Infragravity Waves, *Coastal Engr.* **41**, 467-496.

Westerink, J.J., C.A. Blain, R.A. Luetich, and N.W. Scheffner, 1994a. ADCIRC: An Advanced Three-Dimensional Circulation Model for Shelves, Coasts, and Estuaries, Report 2: User's Manual for ADCIRC-2DDI, Technical Report DRP-92, Department of the Army.

Westerink, J.J., R.A. Luetich, and J.C. Muccino, 1994b. Modeling Tides in the Western North Atlantic Using Unstructured Graded Grids, *Tellus* **46A**, 178-199.

Yu, J., and D.N. Slinn, Effects of Wave-Current Interaction on Rip Currents, 2001, submitted to *J. Geophys. Res.*